Stem Cell Reports
Article

OPEN ACCESS

Long Noncoding RNA Moderates MicroRNA Activity to Maintain Self-Renewal in Embryonic Stem Cells

Keriayn N. Smith,[1] Joshua Starmer,[1] Sarah C. Miller,[1] Praveen Sethupathy,[1] and Terry Magnuson[1,*]
[1]Department of Genetics, University of North Carolina, Chapel Hill, NC 27599, USA
*Correspondence: trm4@med.unc.edu
http://dx.doi.org/10.1016/j.stemcr.2017.05.005

SUMMARY

Of the thousands of long noncoding RNAs expressed in embryonic stem cells (ESCs), few have known roles and fewer have been functionally implicated in the regulation of self-renewal and pluripotency, or the reprogramming of somatic cells to the pluripotent state. In ESCs, *Cyrano* is a stably expressed long intergenic noncoding RNA with no previously assigned role. We demonstrate that *Cyrano* contributes to ESC maintenance, as its depletion results in the loss of hallmarks of self-renewal. Delineation of *Cyrano*'s network through transcriptomics revealed widespread effects on signaling pathways and gene expression networks that contribute to ESC maintenance. *Cyrano* shares unique sequence complementarity with the differentiation-associated microRNA, *mir-7*, and *mir-7* overexpression reduces expression of a key self-renewal factor to a similar extent as *Cyrano* knockdown. This suggests that *Cyrano* functions to restrain the action of *mir-7*. Altogether, we provide a view into the multifaceted function of *Cyrano* in ESC maintenance.

INTRODUCTION

Pluripotent stem cells hold significant therapeutic potential in the context of degenerative disease. To use pluripotent cells in transplantation therapies, a thorough understanding of the molecular mechanisms that regulate immortality through self-renewal becomes a key requirement. The specialized cells that arise from pluripotent cells during development do so through temporal restrictions in their cellular plasticity. The blueprint behind this cell-fate determination is the transcriptome, whose status is based upon regulatory networks consisting of epigenetic machinery, transcription factors, and noncoding RNAs (ncRNAs).

Although well studied, protein-coding sequences account for only approximately 2% of the genome and 28%–40% of the transcriptome in humans (Alexander et al., 2010; Harrow et al., 2012). This suggests that non-protein-coding RNAs may have heretofore unidentified functions. Indeed, it has been demonstrated that ncRNAs are abundant regulatory components of vertebrate transcriptomes. This is particularly evident for long noncoding RNAs (lncRNAs; >200 nt long) and the noncoding class of small RNAs termed microRNAs (miRNAs), which influence numerous biological processes including proliferation, apoptosis, and differentiation.

Mechanistically, lncRNAs have emerged as multifaceted regulators of various cellular processes, with roles that include influencing epigenetic landscapes, transcriptional circuitry, and post-transcriptional regulatory processes (Rinn and Chang, 2012; Wang and Chang, 2011). While lncRNAs generally have no significant open reading frame, many share characteristics of mRNAs such as 5′ capping, splicing, and polyadenylation (Cabili et al., 2011; Guttman et al., 2010). Typically, tissue-specific expression of lncRNAs is more demarcated than that of mRNAs, and it follows that several lncRNAs have been implicated in organ development and cell-fate specification (Fatica and Bozzoni, 2014). These data point to the need for the elucidation of lncRNA function in both specialized and unspecialized cell types.

To date, thousands of lncRNAs have been identified through transcriptomics, particularly RNA sequencing (RNA-seq), in embryonic stem cells (ESCs) (Cabili et al., 2011; Guttman et al., 2010), yet well-defined biological functions are known for very few. However, loss-of-function approaches can provide insight into roles for lncRNAs in the maintenance of self-renewal and pluripotency, reprogramming, and differentiation (Guttman et al., 2011; Kelley and Rinn, 2012; Kim et al., 2015; Lin et al., 2014; Loewer et al., 2010). Such functional characterization would address precise roles for individual lncRNAs in pluripotent stem cell maintenance.

Cyrano (*linc-oip5*, *1700020I14Rik*) is a long intergenic ncRNA (lincRNA) transcribed in mouse ESCs (Chew et al., 2013; Guttman et al., 2010; Ulitsky et al., 2011) that was first characterized in zebrafish (Ulitsky et al., 2011). In zebrafish, it is a key regulator that functions in brain, eye, and nasal development (Ulitsky et al., 2011). This is at least in part mediated by a short region of high sequence conservation among vertebrate genomes that is critical for function. Rescue experiments in zebrafish utilizing higher-order orthologs provided the first insight that *Cyrano* may have a functional role in mice (Ulitsky et al., 2011).

miRNAs, which are much shorter ncRNAs (approximately 22 nt), have also been assigned regulatory roles in numerous biological processes. Historically, miRNAs have been thought to function through pairing with complementary sequences in the 3′ UTR of target mRNAs to

This is an open access article under the CC BY-NC-ND license (http://creativecommons.org/licenses/by-nc-nd/4.0/).

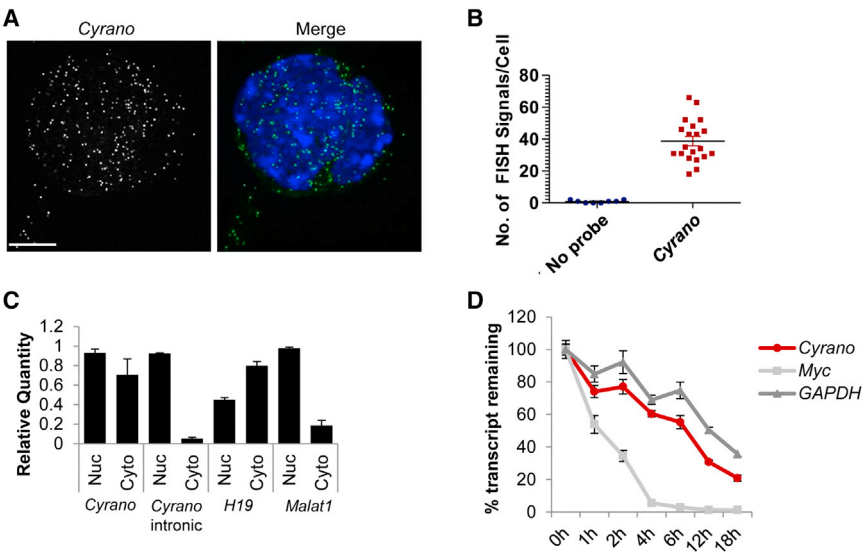

Figure 1. *Cyrano* Displays Dispersed Subcellular Localization and Exhibits Stability in ESCs

(A) smFISH analysis of a representative ESC colony shows *Cyrano* localization in the nucleus and cytoplasm of ESCs. Nuclei, blue (DAPI). Scale bar, 10 μm.

(B) Quantitation of *Cyrano* molecules/ESC.

(C) Subcellular fractionation and qRT-PCR confirms *Cyrano*'s presence in the nucleus and cytoplasm.

(D) Assessment of the stability of *Cyrano*. Data are from three independent experiments. Error bars represent SEM. See also Figure S1.

repress gene expression at the post-transcriptional level (Bartel, 2009). More recently, broader miRNA functionality has been recognized. This includes noncanonical binding to non-3′ UTR regions including the coding sequence of target genes, as well as cross-regulatory interactions that exist between miRNAs and lncRNAs to affect either miRNA or lncRNA stability and/or function, and the regulation of downstream targets (Jeggari et al., 2012; Paraskevopoulou et al., 2013).

One such lncRNA/miRNA interaction has been postulated between *Cyrano* and *mir-7* (Ulitsky et al., 2011). At the cellular level, *mir-7* is associated with differentiation (Cui et al., 2013; Kong et al., 2012; Nguyen et al., 2010), with its levels increasing during neural specification from neural stem cells (Cui et al., 2013). In various cellular contexts, it acts by inhibiting receptor-mediated signaling pathways, including EGFR and STAT3 signaling, to promote differentiation and modulate cellular adhesion (Kefas et al., 2008; Nguyen et al., 2010; Tazawa et al., 2012; Zhang et al., 2014). Antagonism of *mir-7* function, mediated by sequestration and inactivation via molecular sponges or decoy RNAs, is a well-known strategy for moderating its activity on target transcripts. One of the best-studied examples is the circular RNA *CD1Ras/CiRS-7*, which possesses multiple seed matches to *miR-7* (Hansen et al., 2013; Memczak et al., 2013). Sponge-based regulation of miRNA activity is also employed in the ESC regulatory landscape to prevent post-transcriptional degradation of key pluripotency factors including *Oct4*, *Sox2*, and *Nanog* (Wang et al., 2013).

Here, we demonstrate that *Cyrano* is essential for maintenance of self-renewing ESCs. Our studies revealed that interplay between *Cyrano* and *mir-7* affects key properties including cell adhesion in colony maintenance to support ESC immortality. Importantly, *Cyrano* depletion disrupts self-renewal signaling and gene expression regulatory networks, particularly the expression of *Nanog*. Aberrations in these properties including the loss of *Nanog* expression, cell adhesion, and colony survival to maintain self-renewal capacity are recapitulated in *mir-7* gain-of-function experiments. This supports the existence of a competing relationship between *mir-7* and *Cyrano* in ESCs.

RESULTS

lncRNA *Cyrano* Exhibits Stability and Is Broadly Localized in ESCs

While lncRNAs exhibit a range of localization patterns (Cabili et al., 2015), their basic localization provides preliminary insight into their cellular functions. For instance, nuclear-domain localized lncRNAs, including *Xist* and *Kcnq1ot1*, function to silence vast chromatin domains, while the cytoplasmic lncRNA *H19* is a primary miRNA precursor (Cai and Cullen, 2007; Keniry et al., 2012).

To characterize the function of *Cyrano* in ESCs, we first used single-molecule fluorescence in situ hybridization (smFISH) and fractionation methods to examine *Cyrano*'s subcellular localization. Through z-stack imaging of multiple ESC lines, smFISH revealed distinct signals in the nucleus and cytoplasm throughout ESC colonies (Figures 1A and S1A–S1D), averaging ~40 molecules per cell (Figure 1B). This distribution was confirmed by subcellular fractionation comparing the localization of spliced *Cyrano* to the unspliced nuclear form, cytoplasmic *H19* (Keniry et al., 2012) and nuclear speckle-localized *Malat1* (Miyagawa et al., 2012) (Figure 1C). Furthermore, ENCODE data from human ESCs (ENCODE Project Consortium, 2012; Yue et al., 2014) showed similar subcellular

localization of the unspliced and spliced human ortholog, *OIP5-AS1* (Figure S1E). Consistent with the lack of enrichment in either cellular compartment (Clark et al., 2012; Tani et al., 2012), we found that *Cyrano* displayed moderate stability of $t_{1/2}$ ~6 hr in ESCs (Figure 1D). *Cyrano*'s distribution in the cell could indicate that nuclear and cytoplasmic *Cyrano* pools have distinct functions or that it interacts with proteins that shuttle from the nucleus to the cytoplasm.

Cyrano Is Required for Maintenance of ESC Self-Renewal

In addition to consistent localization and expression among ESC lines, microarray analysis of early embryonic developmental stages (Xie et al., 2010) revealed an increase in *Cyrano* expression in morulae and blastocysts relative to two well-studied lncRNAs, *H19* and *Airn* (Figure 2A). Similar results were obtained upon examination of single-cell RNA-seq data (Deng et al., 2014) from ESCs (Figure S2A). ESCs are derived from blastocysts and are an excellent model system for early developmental processes.

We used short hairpin RNA (shRNA) knockdown (KD) to examine the effect of loss of *Cyrano* expression in ESCs. Independent shRNAs reproducibly achieved greater than 60%–85% reduction of *Cyrano* levels (Figures 2B, S2B, and S2C) compared with a nontargeting control (NTC). Within 2–3 days of expression of shRNAs, we found that *Cyrano*-depleted cells were unable to robustly maintain a typical ESC phenotype of tightly packed cells assembled in a dome-shaped colony in leukemia inhibitory factor (LIF)-containing ESC medium (Figure 2C). Because of possible shortcomings in KD efficiency due to multiple lncRNA splice variants, differential subcellular localization, and possible nontargeting of shRNAs, the loss-of-self-renewal phenotype was confirmed using additional shRNAs (Figures S2C and S2D) and in an independent ESC line (Figure S2E). Specifically, we observed increased numbers of cells floating in the medium and prominent partitioning of cell-cell contacts. This is unlike the standard pluripotent ESC state in which cell-cell boundaries within a colony are difficult to define. Along with this breakdown in the colony maintenance of self-renewing ESCs, we observed a sharp reduction in cell numbers in *Cyrano*-depleted cells (Figure 2D). Loss of self-renewal was further underscored by a qualitative and quantitative loss of alkaline phosphatase activity (Figures 2E, 2F, S2D, and S2E) and increases in cell death (Figure 2G). Altogether, these data indicate that *Cyrano* is required for maintenance of ESC self-renewal.

The ESC Gene Expression Signature Is Disrupted by *Cyrano* Deficiency

Pluripotent ESCs are characterized by a well-documented gene expression profile that supports their ability to self-renew while maintaining the capacity for differentiation into embryonic germ layer derivatives (Boyer et al., 2005). We next examined modifications in gene expression profiles upon *Cyrano* KD to determine whether cells assumed a particular cellular identity upon *Cyrano* loss. Total read number in RNA-seq experiments for samples ranged from 23 to 29 million reads, with mapped reads ranging from 88% to 90% of total read number. Concomitant with morphological anomalies, RNA-seq uncovered significant differential gene expression due to shRNA-mediated KD (Figure 3A). Sample comparisons revealed 489 and 380 up- and downregulated genes, respectively, between control and KD samples (Figure 3A). Validation of differentially expressed non-pluripotency-related genes was carried out by qRT-PCR (Figure S3A). Ingenuity Pathway Analysis (IPA) classification revealed that the top dysregulated pathways post KD were primarily related to cell adhesion, signaling, and motility (Figure 3B), observations consistent with the loss-of-function phenotype. Based on these results and phenotypic observations (Figure 2C), we further assessed anomalies in cell adhesion by examining localization of E-cadherin (Figure 3C) and F-actin (Figure S3B) in immunofluorescence assays. E-cadherin is a key pluripotency cell-signaling modulator (Redmer et al., 2011) that typically mediates cell-cell adhesion and is normally found at cell-cell boundaries in ESC colonies. We observed aberrant localization of cell membranous E-cadherin on *Cyrano* depletion (Figure 3C). Furthermore, phalloidin staining (Figure S3B) revealed a loss of F-actin localization as is typically seen at the cell cortex in ESCs (Schratt et al., 2002). In addition to anomalous cell and colony morphology, this uncharacteristic localization of qualitative markers, whose localization is normally indicative of self-renewing ESC colonies, further indicates atypical cell adhesion in colony maintenance.

Cyrano Depletion Disrupts *Nanog* Expression

We next rank-ordered genes that showed a decrease in expression (false discovery rate [FDR] < 0.05). As expected, the reduction in *Cyrano* expression was most significant using this threshold (Figure 4A). Interestingly, the master pluripotency regulator *Nanog* was one of the more significantly downregulated genes (Figure 4A). Further examination of expression of other key factors in self-renewal maintenance (Xu et al., 2014) including *Oct4*, revealed that they remained mostly unchanged while there was a decrease in *Nanog* levels (Figures 4B, S4A–S4D). The specific downregulation of *Nanog* and not other master regulators, including *Oct4*, suggests that *Cyrano* affects a specific subset of self-renewal master genes to result in the observed phenotype, as opposed to being an indirect result of spontaneous differentiation.

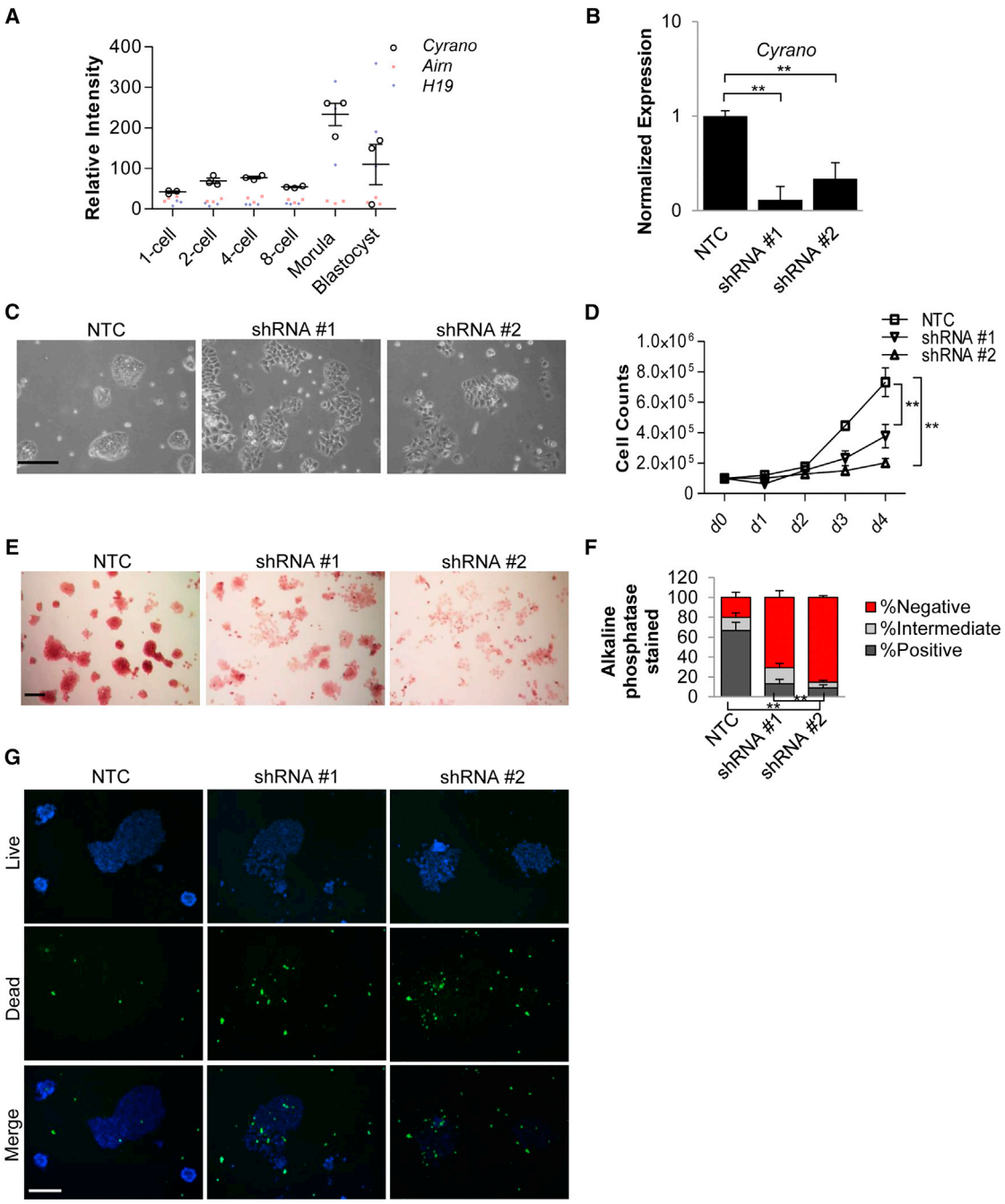

Figure 2. *Cyrano* Deficiency Impairs ESC Self-Renewal

(A) Expression analysis (GEO: GSE18290) of *Cyrano*, *Airn*, and *H19* lncRNAs in early development.

(B) qRT-PCR shows significant reduction in *Cyrano* expression upon KD using independent shRNAs, compared with a nontargeting control. Experiments were performed in triplicate, normalized to *GAPDH*, with error bars representing 95% CI.

(C) *Cyrano* KD results in loss of the ESC characteristic colony morphology. Scale bar, 100 μm.

(D) KD of *Cyrano* results in a decrease in cell numbers as determined by cell counts beginning with plating on day 1 post transfection.

(E and F) Significant reduction in alkaline phosphatase staining of ESC colonies after *Cyrano* KD. n > 200. Scale bar, 100 μm.

(G) Increases in cell death observed upon *Cyrano* KD 2 days post transfection. Nuclei (blue, live; green, dead). Scale bar, 200 μm.

Counts were performed in triplicate with error bars representing SD. Data are from three independent experiments. **p < 0.01. See also Figure S2.

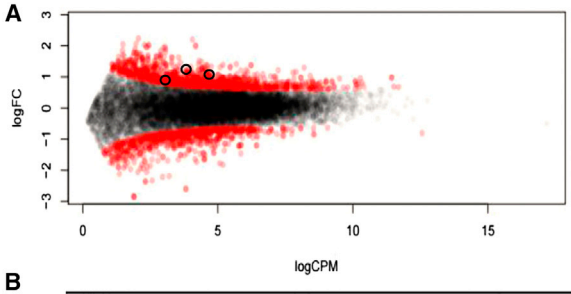

B

Pathway	p-value
Protein Ubiquitination Pathway	0.000115
RhoA Signaling	0.000302
Signaling by Rho Family GTPases	0.000708
Regulation of Actin-based Motility by Rho	0.000891
Epithelial Adherens Junction Signaling	0.001023
Actin Cytoskeleton Signaling	0.005012
EIF2 Signaling	0.006761
RhoGDI Signaling	0.006918
mTOR Signaling	0.008128
Integrin Signaling	0.00871

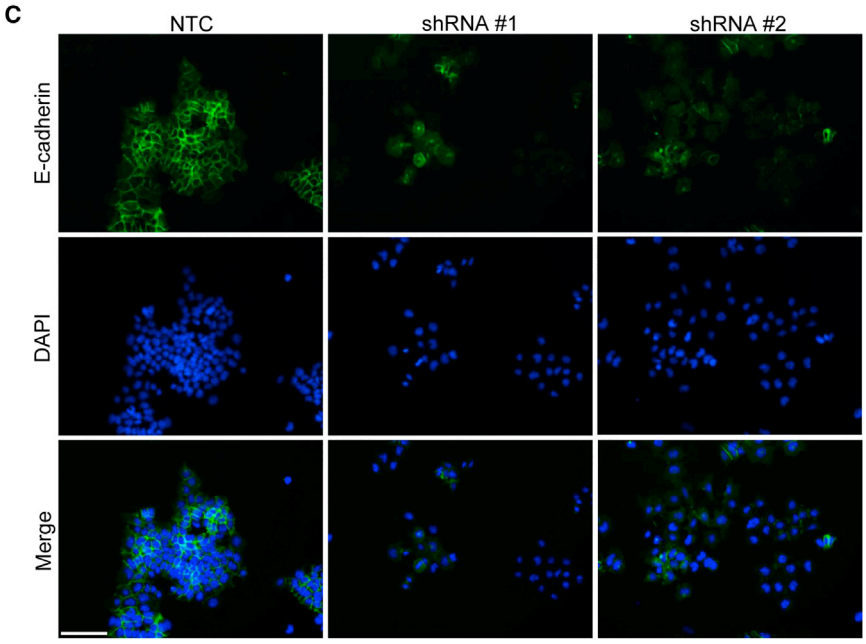

Figure 3. *Cyrano* Depletion Results in Aberrant Gene Expression in ESCs

(A) Smear plot comparing gene expression in NTC and KD samples reveals significant gene expression changes 3 days post KD. Differentially expressed genes are indicated in red, compared with insignificant genes in black (FDR < 0.05).

(B) IPA analysis of differentially expressed genes shows an enrichment of pathways after *Cyrano* KD.

(C) Immunofluorescence examination of E-cadherin in control and KD cells, showing aberrant localization. Nuclei, blue (DAPI); Scale bar, 100 μm.

See also Figure S3.

Aberrant Expression of Anti-Self-Renewal Factors Is Associated with *Cyrano* Depletion

The phenotype upon *Cyrano* loss led us to more closely examine genes that showed significant increases in expression. This revealed key anti-pluripotency genes, including developmental regulators not associated with the ESC state. These include lineage specification markers (*Otx2*, *Nestin*, *Gata4*, *Pdgfra*, and *Sox11*; Figures 4C–4G) and the epithelial-mesenchymal transition factor, *Snai1* (Figure 4H). Furthermore, we observed increases in *Apela* expression (Figure 4I), a recently described regulatory RNA with the ability to encode a small peptide hormone (Chng et al., 2013; Li et al., 2015b; Pauli et al., 2014). The upregulation of *Apela* is consistent with it being a genomic target of *Nanog*, whose expression increases upon RNAi-mediated depletion of *Nanog* (Loh et al., 2006), and its role in mesendoderm specification in zebrafish (Chng et al., 2013). *Apela* expression abruptly increases upon LIF withdrawal in mouse ESCs (Figure S4E), consistent with the reduced capacity to differentiate into mesoderm and

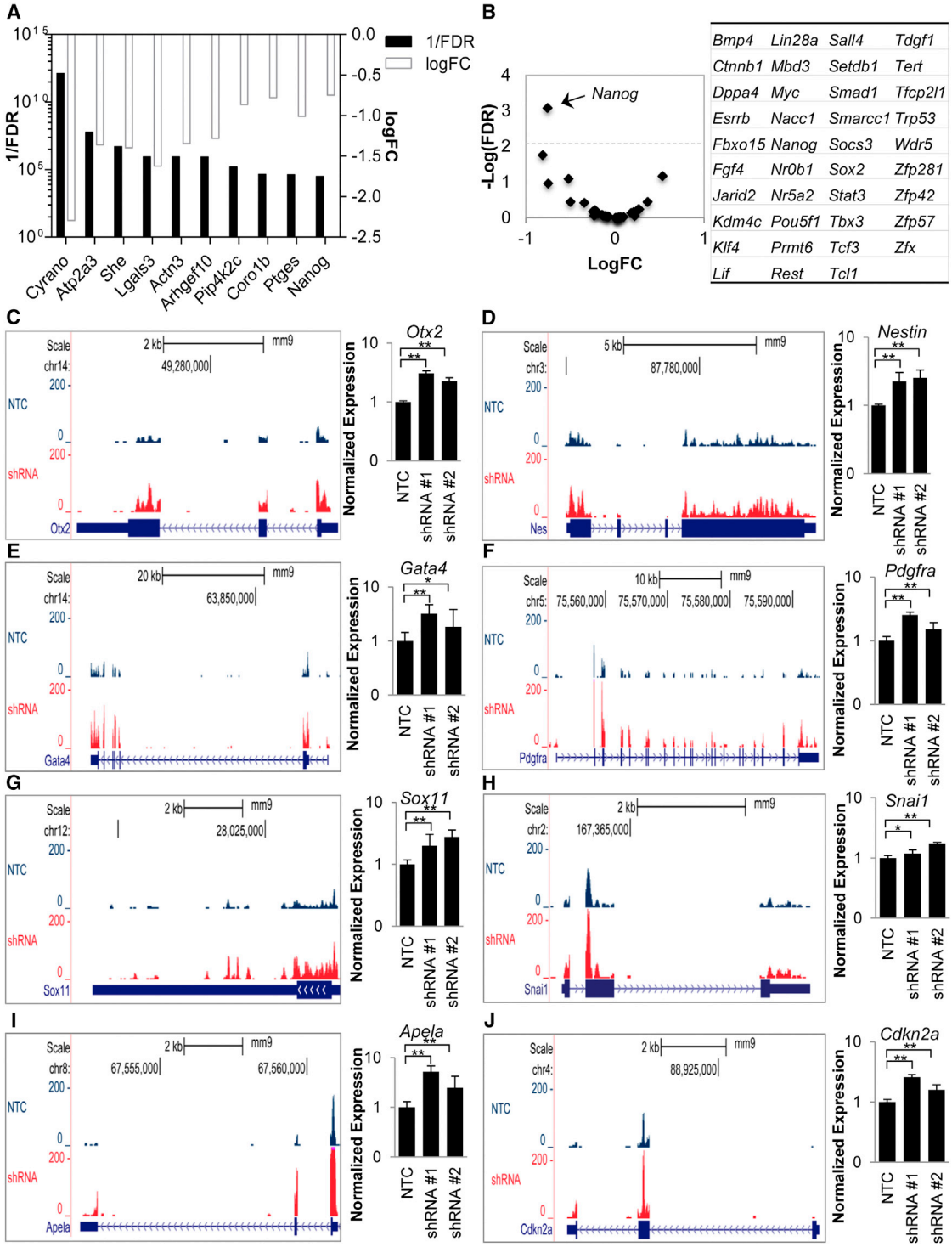

Figure 4. Depletion of *Cyrano* Results in Altered Expression of *Nanog* and Lineage-Related Genes

(A) Ranking of the top-10 decreased genes in RNA-seq based on FDR (black bars) shows significant decreases in *Nanog* levels with *Cyrano* KD. Fold change is also indicated (white bars).

(B) Assessment of pluripotency regulators on *Cyrano* KD reveals that *Nanog* displays the most significant differential regulation.

(legend continued on next page)

endoderm in embryoid bodies with *Apela* depletion (Li et al., 2015b). As *Apela* has been recently shown to be important for self-renewal maintenance in human ESCs (Ho et al., 2015), the rapid upregulation may represent a transition from naive to primed pluripotency prior to spontaneous differentiation. Consistent with this, subsequent downregulation of *Apela* is seen later in mouse ESC differentiation (Figure S4E), similar to the decrease observed in human ESC differentiation (Chng et al., 2013). These results suggest that deviations from ideal *Apela* levels antagonize maintenance of the ESC state.

The constitutive cell cycle of ESCs, which lacks the periodicity of differentiated cell types, is associated with a lack of cyclin D regulation (White and Dalton, 2005). Consistent with the phenotypic change and decreased proliferative capacity, we observed an increase in levels of the cyclin D-Cdk inhibitor, *Cdkn2a*, in *Cyrano*-deficient cells relative to controls (Figure 4J).

Taken together, these gene expression alterations support the failure to retain self-renewal capacity upon *Cyrano* depletion. The function of *Cyrano* does not appear to primarily be via proximal *cis* mechanisms, as no significant gene expression changes were observed in RNA-seq (FDR < 0.05) for neighboring genes within a 100-kb window (Figure S4F), and consistent changes were not observed for both shRNAs in qRT-PCR analyses (Figure S4G).

Cyrano Counteracts *mir-7* Action in ESCs to Support Self-Renewal Maintenance

We sought to determine how *Cyrano* mediates these survival, adhesion, and anti-differentiation roles in ESCs, and hypothesized that *Cyrano* functions were at least partially determined through its unique relationship with *mir-7* (Ulitsky et al., 2011). Several lines of evidence support this hypothesis. (1) In addition to a conventional seed match (Figure S5A and Table S1), the prominently expressed long splice variant (Figure 5A) of *Oip5-AS1*/*Cyrano* (Sigova et al., 2013) possesses an almost complete binding site to *mir-7* in mouse ESCs (Figure 5B) and this binding site is conserved across vertebrates (Figure 5A and Ulitsky et al., 2011). (2) Similar to previous observations in mouse brain (Zhang and Darnell, 2011) and HEK293 (Kishore et al., 2011), *Cyrano* or its human ortholog is bound by Argonaute in ESCs (Figure 5C), similar to the known *mir-7* target gene *Igf1R* (Figure S5B) (Jiang et al., 2010). (3) *mir-7* is associated with differentiation in various cell types (Cui et al., 2013; Kong et al., 2012; Nguyen et al., 2010). (4) *mir-7* is a documented Stat3 pathway antagonist (Zhang et al., 2014) and the LIF-Stat3-Nanog axis is required for mouse ESC self-renewal. (5) Similar to previous observations from Bartel and colleagues, we found that *mir-7* and *Cyrano* physically interact (Figure 5D), as observed for the *mir-7* target *Igf1R* (Jiang et al., 2010) (Figure S5C), suggesting that this molecular interaction could be a mechanism for *Cyrano* regulation of *mir-7* function. Indeed, small RNA-seq data from ENCODE indicated that *mir-7* is expressed and localized similarly to *Cyrano* in ESCs (Figure S5D). Furthermore, nuclear enrichment of *mir-7* has been found in additional contexts including HEK293 and human carcinoma cell lines (Liao et al., 2010), similar to that observed for *Cyrano* (Figures 1A, 1C, and S1A–S1E).

We then determined whether *mir-7* could affect ESC maintenance by downregulating key adhesion and self-renewal regulators. First, we used mirWalk (Dweep and Gretz, 2015) (Figure S5E and Table S2), TargetScan (Agarwal et al., 2015; Lewis et al., 2003, 2005), and RNA22 (Miranda et al., 2006), and found that the 3′ UTR of the ESC-enriched integrin *Itga9* (Nagano et al., 2008; Rugg-Gunn et al., 2012) (Figure 5E) contains a strong 8mer *mir-7* seed sequence. Interestingly, examination of *Nanog*'s 3′ UTR also revealed a 7mer-A1 *mir-7* seed match (Figure 5F). Second, we transfected ESCs with a *mir-7* mimic (Figures 5G, S5F, and S5G) and observed a decrease in *Itga9* (Figure 5H) and *Nanog* levels (Figure 5I). Third, as the *mir-7-Nanog* interaction was based on a weaker prediction, we introduced the *mir-7* mimic along with a luciferase reporter plasmid constituting of the *Nanog* 3′ UTR together with a transfection control and observed inhibition of luciferase expression (Figure S5H). Also, inhibition of *mir-7* resulted in increased *Nanog* levels (Figure S5I). We also found that *Cyrano* levels decreased upon introduction of the *mir-7* mimic, suggesting that *mir-7* also regulates *Cyrano* in ESCs (Figure S5J). Importantly, when we transfected ESCs with the *mir-7* mimic and monitored the ESC phenotype in LIF-containing medium, we observed a loss of ESC colony maintenance within 2 days of *mir-7* introduction (Figure 5J). This was accompanied by anomalies in cell and colony adhesion with numerous detached cells (Figure 5J) and increases in cell death (Figure 5K), similar to observations made upon *Cyrano* depletion. Finally, as *Itga9* and *Nanog* levels decreased upon *mir-7* overexpression as well as upon *Cyrano* depletion (Figures S5K and S4B–S4D), we hypothesized that *Itga9* and *Nanog* levels would increase with modulation of *Cyrano* levels and found that increased expression of *Cyrano* (Figure 5L) augmented their

(C–J) UCSC genome browser plots shows RNA-seq reads mapped to mm9 and normalized to remove sequencing depth biases, and independent qRT-PCR examination upon *Cyrano* KD indicates increased expression of factors that antagonize self-renewal in mouse ESCs. Data are from three independent experiments with error bars representing 95% CI. *p < 0.05, **p < 0.01.
See also Figure S4.

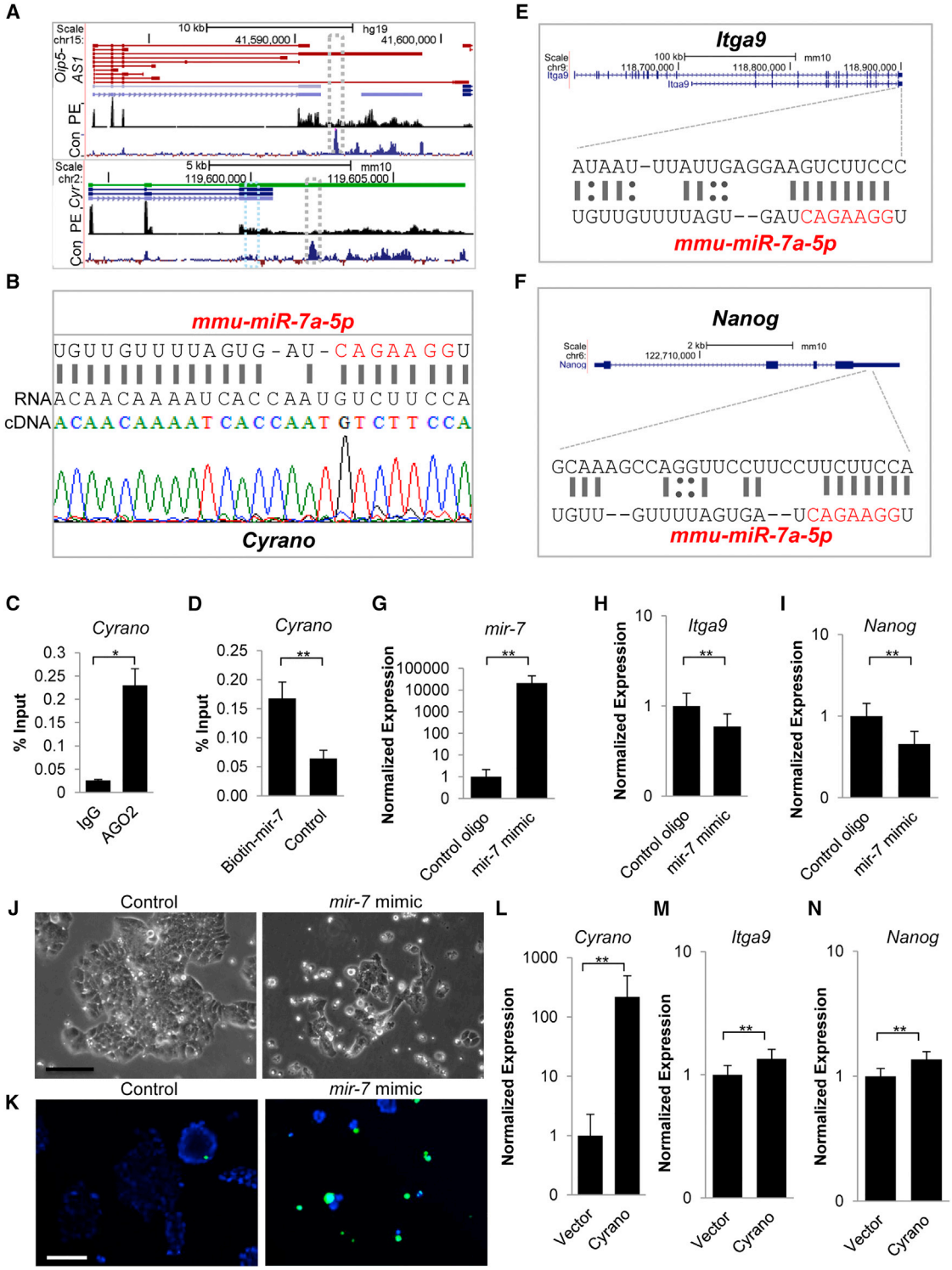

Figure 5. *Cyrano* Restrains *mir-7* Activity to Support ESC Self-Renewal

(A) Genome browser blots showing *Oip5-AS1/Cyrano* splice variants. Despite the presence of multiple splice variants of *Oip5-AS1*, the long variant containing the conserved *mir-7* binding site (gray box; segment of this region with the *mir-7* interaction site is expanded in B) is prominently expressed in human ESCs (top panel, GEO: GSE41009) and mouse ESCs (bottom panel, GEO: GSE36799). Blue box marks

(legend continued on next page)

expression (Figures 5M and 5N). This suggests that *Cyrano* and *mir-7* act in opposition to one another in ESCs.

It is now well established that compared with culture in serum + LIF, mouse ESCs can be cultured more homogenously in the presence of GSK3 and MEK inhibitors (2i, Ying et al., 2008). Due to the heterogeneity observed in serum + LIF, we also tested the effect of *Cyrano* depletion under conditions of more homogeneity. Under 2i conditions, *Nanog* expression is somewhat higher than that of growth conditions in serum-containing medium (Abranches et al., 2014), whereas *Cyrano*'s levels remain unchanged (Figure S6). To further delineate whether *Cyrano* functions upstream of *Nanog*, we examined the effect of *Cyrano* KD in ESCs under conditions of higher *Nanog* expression: (1) cells cultured in 2i and (2) *Nanog* overexpression. Similar to observations in serum-containing LIF medium, KD of *Cyrano* in 2i resulted primarily in a loss of self-renewal maintenance, and increased *Nanog* expression resulted in partial recovery of self-renewal capacity (Figures 6A–6D). This suggests that additional mechanisms of *Cyrano* action are functional in ESC maintenance. Delineation of *Cyrano* function can be further enhanced through single-cell analyses of ESC lines harboring endogenously encoded reporters and mutant alleles of *Cyrano* and putative direct and indirect targets.

Altogether, we provide evidence for *Cyrano*'s role in cell survival and colony maintenance in self-renewing ESCs. Furthermore, our results provide evidence for one direct mechanism by which *Cyrano* functions, namely the existence of a negative-feedback loop between *Cyrano* and *mir-7* (see Graphical Abstract), to support the maintenance of ESC self-renewal through factors including *Nanog* and *Itga9* that sustain key properties of pluripotent cells.

DISCUSSION

Of the nearly 9,000 known lncRNAs (Derrien et al., 2012; Harrow et al., 2006, 2012), the mechanism of action is understood for only a small fraction. We have described a previously undefined role for *Cyrano* in the maintenance of the self-renewing state of mammalian pluripotent cells, a model cell type for establishing mechanisms of action relevant to early development and regenerative medicine.

In our characterization of *Cyrano* function, we show that depletion of *Cyrano* results in disarray in the pluripotent gene expression signature and defects in self-renewal maintenance. Driving this is aberrations in colony survival and preservation, which requires maintenance of cellular adhesion and signaling, as well as the decrease in *Nanog* expression, which itself is required for cell growth and apoptosis avoidance in ESCs (Chen et al., 2012). Furthermore, it is well established that *Nanog* function has far-reaching implications in the repression of negative regulators of the ESC state, such as *Dkk1* and *Gata6* (Loh et al., 2006; Singh et al., 2007). Mining gene expression data produced in a recent shRNA screen for lncRNAs that regulate pluripotency further supports *Cyrano*'s key role (Lin et al., 2014).

Misregulation and aberrant expression of lncRNAs are increasingly associated with disease states (Wapinski and Chang, 2011; Batista and Chang, 2013; Fatica and Bozzoni, 2014). Similar signaling pathways (e.g., Jak-Stat, PI3K/AKT) and transcription factors (e.g., Myc, Stat3) activities support stem cell growth and survival as well as tumorigenesis (Kim et al., 2010). As *Cyrano* displays particularly high expression in ENCODE cancer cell lines, a priority will be to determine the requirement of *Cyrano* in tumor cell survival and cellular reprogramming to a malignant state. Indeed, similar to our findings in ESCs, *Cyrano* supports glioma cell proliferation in addition to cell migration and tumorigenesis (Hu et al., 2017).

Complex relationships exist between miRNAs and lncRNAs in transcriptional, post-transcriptional, and translational regulatory processes. Previous studies have shown that lncRNAs can function as miRNA precursors and miRNA targets, or compete as decoys/sponges/competing

additional conventional *mir-7* seed sequence. Con denotes conservation: Vertebrate Multiz Alignment & Conservation; PE, paired-end RNA-seq; Cyr, *Cyrano*.

(B) Near-complete *mir-7* sequence complementarity is observed in *Cyrano* sequenced from ESCs.

(C) RNA immunoprecipitation indicates that *Cyrano* is bound by Ago2 in ESCs. Experiments were performed in triplicate with error bars representing SEM.

(D) miRNA pull-down and qPCR indicates a physical interaction between *Cyrano* and *mir-7*. Experiments were performed in triplicate with error bars representing SEM.

(E and F) The 3′ UTRs of *Itga9* and *Nanog* contain *mir-7* target sites (see Figure S5; Tables S1 and S2 for further information on target sites).

(G–N) Overexpression of *mir-7* (G) results in a decrease in *Itga9* (H) and *Nanog* levels (I), loss of ESC self-renewal maintenance (J), and increased cell death (K) in ESCs 2 days post transfection. Nuclei (blue, live; green, dead); Scale bar, 100 μm. qRT-PCR monitoring of *Cyrano* (L), *Itga9* (M), and *Nanog* (N) levels with *Cyrano* overexpression. Error bars for qRT-PCR expression analysis represent 95% CI.

Data are from three independent experiments. *$p < 0.05$, **$p < 0.01$. See also Figure S5; Tables S1 and S2.

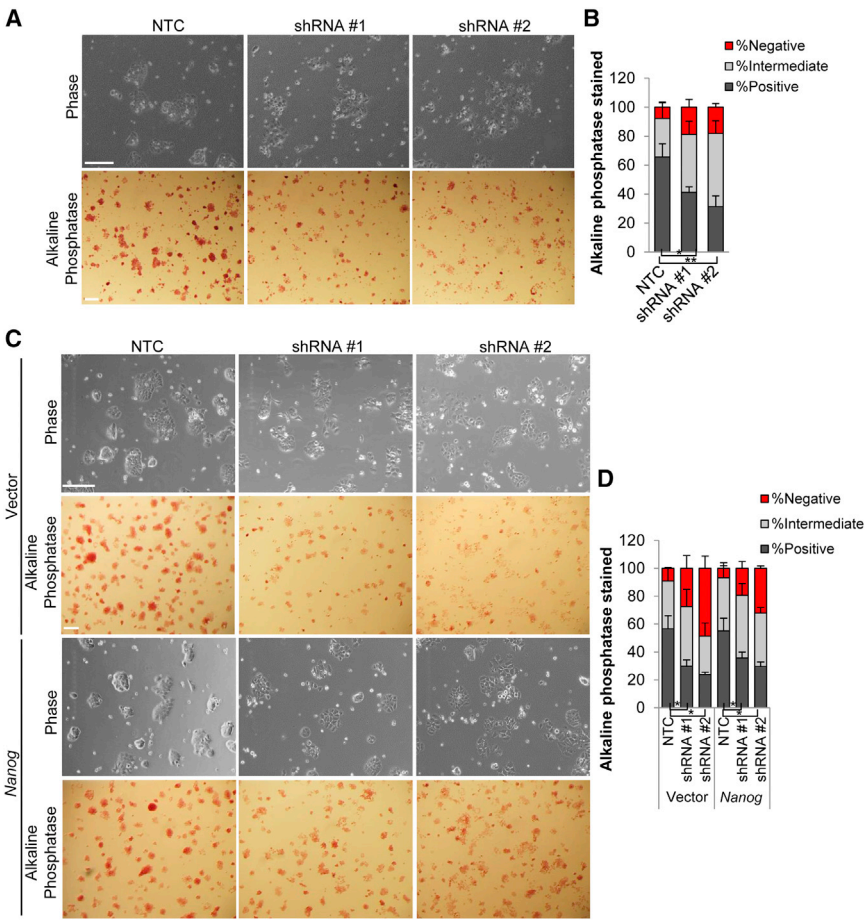

Figure 6. Ability of Increased *Nanog* Expression to Rescue the *Cyrano* KD Phenotype

(A and B) A reduction in alkaline phosphatase staining is observed in ESC colonies after *Cyrano* KD in 2i medium.

(C and D) *Nanog* overexpression results in qualitative/partial rescue of *Cyrano* KD phenotype. n > 120.

Scale bar, 100 μm. Data are from three independent experiments and error bars represent SD. *p < 0.05, **p < 0.01. See also Figure S6.

endogenous RNAs to prevent inhibition of mRNA targets (Jeggari et al., 2012; Paraskevopoulou et al., 2013). In the context of skeletal muscle differentiation, *H19* antagonizes *let-7*, releasing the repression of *let-7* targets such as *HMGA2* (Kallen et al., 2013). Similarly, if *Cyrano* has a negative influence on *mir-7* function, it would be expected that depletion of *Cyrano* would free *mir-7* to repress its targets, while overexpression of *Cyrano* would boost *mir-7* target-transcript levels, consistent with our observations.

Moreover, the combination of multiple sites for binding to *Cyrano*, including the unique ultra-conserved binding site, along with the intermediate expression of *mir-7* in ESCs (Tang et al., 2006), suggests that it is feasible for *Cyrano* to attenuate *mir-7* activity to sustain self-renewal. This is particularly relevant for supporting the maintenance of expression of targets such as *Nanog*, which display some heterogeneity in expression in ESCs (Abranches et al., 2014; Singh et al., 2007). While *Nanog* transcripts range from 0 to 500 mRNA molecules per ESC in normal culture conditions, a fraction of pluripotent cells exhibit low *Nanog* expression in the range of <25 molecules/cell (Abranches et al., 2014). One hypothesis is that *Cyrano* is one factor that presents a barrier to lineage commitment in conditions of suboptimal fluctuations in *Nanog* levels. Additionally or alternatively, *Cyrano* may also directly repress lineage specification factors. Further studies may reveal mechanisms behind the molecular interplay between *Cyrano* and its interacting RNAs at the single-molecule and single-cell levels.

Based on our and previously available data, we postulate that regulating RNAs and proteins through interactions is a prominent role of the 8.2-kb *Cyrano* molecule. Indeed, the ortholog *OIP5-AS1* has been found to bind 37 RNA binding proteins (RBPs) (Li et al., 2015a), and a recent report provided further evidence for *Cyrano*'s interaction with other RNAs and highlighted the capacity for *Cyrano* to function as a sponge of RBPs from mRNAs (Kim et al., 2016). Overall, our observations along with other emerging data on *Cyrano*, which in various systems include anti-proliferative functions and roles in organogenesis/embryonic development, are strongly indicative of complex biological function, which clearly warrants further study.

EXPERIMENTAL PROCEDURES

Cell Culture and RNAi

Mouse R1 (XY, Nagy et al., 1993) ESCs were maintained in complete medium supplemented with LIF on gelatin-coated dishes. Mouse ES2-1 (XX, Royce-Tolland et al., 2010) were maintained in complete medium with LIF on feeders or gelatin-coated dishes. Embryoid body differentiation was carried out on low adherent dishes under LIF withdrawal conditions.

RNA Extraction and qRT-PCR

Total RNA was isolated using the RNeasy Mini Kit (Qiagen) or the Quick-RNA MiniPrep Kit (Zymo), followed by DNase treatment (Ambion) and reverse transcription using the iScript reagent (Bio-Rad). qRT-PCR for lncRNA and mRNA transcripts was performed using primers listed in Table S3 with the SsoFast Evagreen Supermix (Bio-Rad) or Taqman Assays (Applied Biosystems).

miRNAs were extracted with the Quick-RNA MiniPrep Kit (Zymo) and reverse transcription carried out with the TaqMan MicroRNA Reverse Transcription Kit. *miR-7* and the *U6* control were amplified using the TaqMan Universal Master Mix II, no UNG and TaqMan microRNA assays for *mmu-miR-7a-5p* and *U6*, respectively.

Data were analyzed based on the $2^{-\Delta\Delta Ct}$, after log transformation, mean centering, and autoscaling (Willems et al., 2008). For these and other quantitative data, experiments were carried out in at least three independent replicates and unpaired, two-tailed Student's t-tests used to determine statistical significance (**$p < 0.01$, *$p < 0.05$, $^{\dagger}p < 0.1$ in figures).

Alkaline Phosphatase Assay

Alkaline phosphatase activity was detected using a leukocyte alkaline phosphatase staining kit (Sigma), and the effect of *Cyrano* KD assessed on day 3 post-transfection.

smFISH

A pool of 36 FISH probes for *Cyrano* was used for hybridization (Biosearch Technologies) for cells cultured on coverslips for approximately 24–30 hr. After fixing with 4% paraformaldehyde (PFA) and permeabilization, cells were hybridized in 100 mg/mL dextran sulfate, 1% formamide, and 2× saline sodium citrate overnight at 37°C.

Transcriptomics

Libraries for RNA-seq were prepared from total RNA with a modified dUTP strand-specific method (Zhong et al., 2011). RNA-seq reads were aligned to the mm9 mouse genome using TopHat (Trapnell et al., 2009) and reads per gene were counted using HTSeq-count (Anders et al., 2015). Normalized bedgraphs were generated for the UCSC genome browser using bedtools (Quinlan and Hall, 2010). Differential expression between NTC and shRNA KD was performed using edgeR (Robinson et al., 2010) after removing genes with fewer than 20 reads, mapping to them across all replicates. Expression changes were visualized using ggplot2 (Wickham, 2009).

Publicly available microarray data (GEO: GSE18290) (Xie et al., 2010) of 1-cell, 2-cell, 4-cell, 8-cell, morula, and blastocyst embryos were used to examine the expression of *Cyrano*, Airn, and H19 lncRNAs. Publicly available data (GEO: GSE45719, Deng et al., 2014) were used for single-cell RNA-seq analysis of *Cyrano* (1700020I14Rik) expression in preimplantation embryos.

Publicly available paired-end RNA-seq data (GEO: GSE36799, GSE41009; Sigova et al., 2013) were used to examine expression of *Cyrano* splice variants in mouse and human ESCs.

RNA Immunoprecipitation and miRNA Target Isolation

Coimmunoprecipitation of Argonaute-bound RNAs was performed generally as previously described (Moran et al., 2012). Ago2 antibody (04-642, Millipore) or immunoglobulin G control was coupled to protein A/G magnetic beads (Thermo Fisher) and incubated with cellular lysate prepared from approximately 1.0×10^7 cells previously crosslinked with 0.3% formaldehyde. Immunoprecipitation was carried out overnight at 4°C with gentle rotation followed by extensive washes. RNA was eluted in the presence of proteinase K and incubated at 65°C for 2 hr to reverse crosslinks. RNA was purified using the RNA Clean & Concentrator Kit (Zymo) followed by reverse transcription (iScript, Bio-Rad) for use in qPCR.

Cells for miRNA pull-down were transfected with biotin-tagged *mir-7* at a concentration of 50 nM and harvested approximately 30 hr post transfection. Cleared cellular lysate was incubated with streptavidin-magnetic beads preblocked with RNase-free BSA and yeast tRNA for 1 hr at 4°C. After washing, RNA was isolated with TRIzol, followed by reverse transcription (iScript) for use in qPCR.

Western Blot Analysis and Immunofluorescence

Antibodies were used for lamin A/C (E-1, sc-376248, Santa Cruz Biotechnology), Oct4 (C-10, sc-5279, Santa Cruz), Nanog (A300-397A, Bethyl Laboratories; #8822, Cell Signaling Technologies), E-cadherin (13-1900, Zymed), and β-actin (ab8226, Abcam) on cell extracts prepared using a modified RIPA buffer or fixed for immunofluorescence experiments with 4% PFA.

miRNA Binding Site Prediction and Luciferase Assays

miRNA binding sites for *Itga9* and *Nanog* were predicted using miRWalk (Dweep and Gretz, 2015), TargetScan (Agarwal et al., 2015; Lewis et al., 2003, 2005), and RNA22 (Miranda et al., 2006). Cells were cotransfected in 24-well plates using Lipofectamine 3000 (Thermo Fisher) for Dual-Luciferase Reporter Assays (Promega) according to the manufacturer's protocol. miRNA mimics (50 nM, Dharmacon) were introduced along with 50 ng of the firefly luciferase vector pGL3 containing the *Nanog* 3′ UTR (Luc-Nanog-3′ UTR was a gift from Lin He, Addgene plasmid #63893) (Choi et al., 2011) and 5 ng of the control Renilla luciferase vector, pRL-TK (Promega). Firefly luciferase and Renilla luciferase activities were consecutively measured 48 hr post transfection.

ACCESSION NUMBERS

Gene expression data are publicly available and can be retrieved from the GEO, NCBI under accession number GEO: GSE98297.

SUPPLEMENTAL INFORMATION

Supplemental Information includes Supplemental Experimental Procedures, six figures, and three tables and can be found with this article online at http://dx.doi.org/10.1016/j.stemcr.2017.05.005.

AUTHOR CONTRIBUTIONS

Conceptualization, K.N.S. and T.M.; Methodology, K.N.S. and J.S.; Investigation, K.N.S. and S.C.M.; Formal Analysis, K.N.S, J.S. and T.M.; Data Curation, J.S.; Writing – Original Draft, K.N.S.; Writing – Review & Editing, K.N.S., J.S., S.C.M., P.S., and T.M.; Funding Acquisition, T.M.; Resources, P.S. and T.M.; Supervision, K.N.S and T.M.

ACKNOWLEDGMENTS

We thank Dr. Barbara Panning for the ES2-1 line, Dr. Mauro Calabrese for helpful discussions and critical comments on the manuscript, and the members of the T.M. laboratory for comments. Grant support: NIH R01 GM101974 to T.M.

Received: August 14, 2016
Revised: May 2, 2017
Accepted: May 3, 2017
Published: June 1, 2017

REFERENCES

Abranches, E., Guedes, A.M., Moravec, M., Maamar, H., Svoboda, P., Raj, A., and Henrique, D. (2014). Stochastic NANOG fluctuations allow mouse embryonic stem cells to explore pluripotency. Development *141*, 2770–2779.

Agarwal, V., Bell, G.W., Nam, J., and Bartel, D.P. (2015). Predicting effective microRNA target sites in mammalian mRNAs. Elife *4*, e05005.

Alexander, R.P., Fang, G., Rozowsky, J., Snyder, M., and Gerstein, M.B. (2010). Annotating non-coding regions of the genome. Nat. Rev. Genet. *11*, 559–571.

Anders, S., Pyl, P.T., and Huber, W. (2015). HTSeq—a Python framework to work with high-throughput sequencing data. Bioinformatics *31*, 166–169.

Bartel, D.P. (2009). MicroRNAs: target recognition and regulatory functions. Cell *136*, 215–233.

Batista, P.J., and Chang, H.Y. (2013). Long noncoding RNAs: cellular address codes in development and disease. Cell *152*, 1298–1307.

Boyer, L.A., Lee, T.I., Cole, M.F., Johnstone, S.E., Levine, S.S., Zucker, J.P., Guenther, M.G., Kumar, R.M., Murray, H.L., Jenner, R.G., et al. (2005). Core transcriptional regulatory circuitry in human embryonic stem cells. Cell *122*, 947–956.

Cabili, M.N., Trapnell, C., Goff, L., Koziol, M., Tazon-Vega, B., Regev, A., and Rinn, J.L. (2011). Integrative annotation of human large intergenic noncoding RNAs reveals global properties and specific subclasses. Genes Dev. *25*, 1915–1927.

Cabili, M.N., Dunagin, M.C., McClanahan, P.D., Biaesch, A., Padovan-Merhar, O., Regev, A., Rinn, J.L., and Raj, A. (2015). Localization and abundance analysis of human lncRNAs at single-cell and single-molecule resolution. Genome Biol. *16*, 20.

Cai, X., and Cullen, B.R. (2007). The imprinted H19 noncoding RNA is a primary microRNA precursor. RNA *13*, 313–316.

Chen, T., Du, J., and Lu, G. (2012). Cell growth arrest and apoptosis induced by Oct4 or Nanog knockdown in mouse embryonic stem cells: a possible role of Trp53. Mol. Biol. Rep. *39*, 1855–1861.

Chew, G.L., Pauli, A., Rinn, J.L., Regev, A., Schier, A.F., and Valen, E. (2013). Ribosome profiling reveals resemblance between long non-coding RNAs and 5′ leaders of coding RNAs. Development *140*, 2828–2834.

Chng, S.C., Ho, L., Tian, J., and Reversade, B. (2013). ELABELA: a hormone essential for heart development signals via the apelin receptor. Dev. Cell *27*, 672–680.

Choi, Y.J., Lin, C., Ho, J.J., He, X., Okada, N., Bu, P., Zhong, Y., Kim, S.Y., Bennett, M.J., Chen, C., et al. (2011). miR-34 miRNAs provide a barrier for somatic cell reprogramming. Nat. Cell Biol. *13*, 1353–1360.

Clark, M.B., Johnston, R.L., Inostroza-Ponta, M., Fox, A.H., Fortini, E., Moscato, P., Dinger, M.E., and Mattick, J.S. (2012). Genome-wide analysis of long noncoding RNA stability. Genome Res. *22*, 885–898.

Cui, Y., Xiao, Z., Chen, T., Wei, J., Chen, L., Liu, L., Chen, B., Wang, X., Li, X., and Dai, J. (2013). The miR-7 identified from collagen biomaterial-based three-dimensional cultured cells regulates neural stem cell differentiation. Stem Cells Dev. *23*, 393–405.

Deng, Q., Ramsköld, D., Reinius, B., and Sandberg, R. (2014). Single-cell RNA-seq reveals dynamic, random monoallelic gene expression in mammalian cells. Science *343*, 193–196.

Derrien, T., Johnson, R., Bussotti, G., Tanzer, A., Djebali, S., Tilgner, H., Guernec, G., Martin, D., Merkel, A., Knowles, D.G., et al. (2012). The GENCODE v7 catalog of human long noncoding RNAs: analysis of their gene structure, evolution, and expression. Genome Res. *22*, 1775–1789.

Dweep, H., and Gretz, N. (2015). miRWalk2. 0: a comprehensive atlas of microRNA-target interactions. Nat. Methods *12*, 697.

ENCODE Project Consortium (2012). An integrated encyclopedia of DNA elements in the human genome. Nature *489*, 57–74.

Fatica, A., and Bozzoni, I. (2014). Long non-coding RNAs: new players in cell differentiation and development. Nat. Rev. Genet. *15*, 7–21.

Guttman, M., Garber, M., Levin, J.Z., Donaghey, J., Robinson, J., Adiconis, X., Fan, L., Koziol, M.J., Gnirke, A., Nusbaum, C., et al. (2010). Ab initio reconstruction of cell type-specific transcriptomes in mouse reveals the conserved multi-exonic structure of lincRNAs. Nat. Biotechnol. *28*, 503–510.

Guttman, M., Donaghey, J., Carey, B.W., Garber, M., Grenier, J.K., Munson, G., Young, G., Lucas, A.B., Ach, R., Bruhn, L., et al. (2011). lincRNAs act in the circuitry controlling pluripotency and differentiation. Nature *477*, 295–300.

Hansen, T.B., Jensen, T.I., Clausen, B.H., Bramsen, J.B., Finsen, B., Damgaard, C.K., and Kjems, J. (2013). Natural RNA circles function as efficient microRNA sponges. Nature *495*, 384–388.

Harrow, J., Denoeud, F., Frankish, A., Reymond, A., Chen, C.K., Chrast, J., Lagarde, J., Gilbert, J.G., Storey, R., Swarbreck, D., et al. (2006). GENCODE: producing a reference annotation for ENCODE. Genome Biol. *7* (*Suppl 1*), S4.1–S4.9.

Harrow, J., Frankish, A., Gonzalez, J.M., Tapanari, E., Diekhans, M., Kokocinski, F., Aken, B.L., Barrell, D., Zadissa, A., Searle, S., et al. (2012). GENCODE: the reference human genome annotation for the ENCODE Project. Genome Res. *22*, 1760–1774.

Ho, L., Tan, S.Y., Wee, S., Wu, Y., Tan, S.J., Ramakrishna, N.B., Chng, S.C., Nama, S., Sczerbinska, I., Chan, Y., et al. (2015). ELABELA is an endogenous growth factor that sustains hESC self-renewal via the PI3K/AKT pathway. Cell Stem Cell *17*, 435–447.

Hu, G., Wu, L., Kuang, W., Chen, Y., Zhu, X., Guo, H., and Lang, H. (2017). Knockdown of linc-OIP5 inhibits proliferation and migration of glioma cells through down-regulation of YAP-NOTCH signaling pathway. Gene *610*, 24–31.

Jeggari, A., Marks, D.S., and Larsson, E. (2012). miRcode: a map of putative microRNA target sites in the long non-coding transcriptome. Bioinformatics *28*, 2062–2063.

Jiang, L., Liu, X., Chen, Z., Jin, Y., Heidbreder, C.E., Kolokythas, A., Wang, A., Dai, Y., and Zhou, X. (2010). MicroRNA-7 targets IGF1R (insulin-like growth factor 1 receptor) in tongue squamous cell carcinoma cells. Biochem. J. *432*, 199–205.

Kallen, A.N., Zhou, X., Xu, J., Qiao, C., Ma, J., Yan, L., Lu, L., Liu, C., Yi, J., Zhang, H., et al. (2013). The imprinted H19 lncRNA antagonizes let-7 microRNAs. Mol. Cell *52*, 101–112.

Kefas, B., Godlewski, J., Comeau, L., Li, Y., Abounader, R., Hawkinson, M., Lee, J., Fine, H., Chiocca, E.A., Lawler, S., and Purow, B. (2008). microRNA-7 inhibits the epidermal growth factor receptor and the Akt pathway and is down-regulated in glioblastoma. Cancer Res. *68*, 3566–3572.

Kelley, D., and Rinn, J. (2012). Transposable elements reveal a stem cell-specific class of long noncoding RNAs. Genome Biol. *13*, R107.

Keniry, A., Oxley, D., Monnier, P., Kyba, M., Dandolo, L., Smits, G., and Reik, W. (2012). The H19 lincRNA is a developmental reservoir of miR-675 that suppresses growth and Igf1r. Nat. Cell Biol. *14*, 659–665.

Kim, J., Woo, A.J., Chu, J., Snow, J.W., Fujiwara, Y., Kim, C.G., Cantor, A.B., and Orkin, S.H. (2010). A Myc network accounts for similarities between embryonic stem and cancer cell transcription programs. Cell *143*, 313–324.

Kim, D.H., Marinov, G.K., Pepke, S., Singer, Z.S., He, P., Williams, B., Schroth, G.P., Elowitz, M.B., and Wold, B.J. (2015). Single-cell transcriptome analysis reveals dynamic changes in lncRNA expression during reprogramming. Cell Stem Cell *16*, 88–101.

Kim, J., Abdelmohsen, K., Yang, X., De, S., Grammatikakis, I., Noh, J.H., and Gorospe, M. (2016). LncRNA OIP5-AS1/cyrano sponges RNA-binding protein HuR. Nucleic Acids Res. *44*, 2378–2392.

Kishore, S., Jaskiewicz, L., Burger, L., Hausser, J., Khorshid, M., and Zavolan, M. (2011). A quantitative analysis of CLIP methods for identifying binding sites of RNA-binding proteins. Nat. Methods *8*, 559–564.

Kong, D., Piao, Y., Yamashita, S., Oshima, H., Oguma, K., Fushida, S., Fujimura, T., Minamoto, T., Seno, H., Yamada, Y., et al. (2012). Inflammation-induced repression of tumor suppressor miR-7 in gastric tumor cells. Oncogene *31*, 3949–3960.

Lewis, B.P., Shih, I., Jones-Rhoades, M.W., Bartel, D.P., and Burge, C.B. (2003). Prediction of mammalian microRNA targets. Cell *115*, 787–798.

Lewis, B.P., Burge, C.B., and Bartel, D.P. (2005). Conserved seed pairing, often flanked by adenosines, indicates that thousands of human genes are microRNA targets. Cell *120*, 15–20.

Li, J., Liu, S., Zheng, L., Wu, J., Sun, W., Wang, Z., Zhou, H., Qu, L., and Yang, J. (2015a). Discovery of protein-lncRNA interactions by integrating large-scale CLIP-seq and RNA-seq datasets. Front. Bioeng. Biotechnol. *2*, 88.

Li, M., Gou, H., Tripathi, B.K., Huang, J., Jiang, S., Dubois, W., Waybright, T., Lei, M., Shi, J., Zhou, M., et al. (2015b). An apela RNA-containing negative feedback loop regulates p53-mediated apoptosis in embryonic stem cells. Cell Stem Cell *16*, 669–683.

Liao, J., Ma, L., Guo, Y., Zhang, Y., Zhou, H., Shao, P., Chen, Y., and Qu, L. (2010). Deep sequencing of human nuclear and cytoplasmic small RNAs reveals an unexpectedly complex subcellular distribution of miRNAs and tRNA 3′ trailers. PLoS One *5*, e10563.

Lin, N., Chang, K., Li, Z., Gates, K., Rana, Z.A., Dang, J., Zhang, D., Han, T., Yang, C., and Cunningham, T.J. (2014). An evolutionarily conserved long noncoding RNA TUNA controls pluripotency and neural lineage commitment. Mol. Cell *53*, 1005–1019.

Loewer, S., Cabili, M.N., Guttman, M., Loh, Y., Thomas, K., Park, I.H., Garber, M., Curran, M., Onder, T., Agarwal, S., et al. (2010). Large intergenic non-coding RNA-RoR modulates reprogramming of human induced pluripotent stem cells. Nat. Genet. *42*, 1113–1117.

Loh, Y., Wu, Q., Chew, J., Vega, V.B., Zhang, W., Chen, X., Bourque, G., George, J., Leong, B., Liu, J., et al. (2006). The Oct4 and Nanog transcription network regulates pluripotency in mouse embryonic stem cells. Nat. Genet. *38*, 431–440.

Memczak, S., Jens, M., Elefsinioti, A., Torti, F., Krueger, J., Rybak, A., Maier, L., Mackowiak, S.D., Gregersen, L.H., Munschauer, M., et al. (2013). Circular RNAs are a large class of animal RNAs with regulatory potency. Nature *495*, 333–338.

Miranda, K.C., Huynh, T., Tay, Y., Ang, Y., Tam, W., Thomson, A.M., Lim, B., and Rigoutsos, I. (2006). A pattern-based method for the identification of MicroRNA binding sites and their corresponding heteroduplexes. Cell *126*, 1203–1217.

Miyagawa, R., Tano, K., Mizuno, R., Nakamura, Y., Ijiri, K., Rakwal, R., Shibato, J., Masuo, Y., Mayeda, A., Hirose, T., and Akimitsu, N. (2012). Identification of cis- and trans-acting factors involved in the localization of MALAT-1 noncoding RNA to nuclear speckles. RNA *18*, 738–751.

Moran, V.A., Niland, C.N., and Khalil, A.M. (2012). Co-immunoprecipitation of long noncoding RNAs. Methods Mol. Biol. *925*, 219–228.

Nagano, K., Yoshida, Y., and Isobe, T. (2008). Cell surface biomarkers of embryonic stem cells. Proteomics *8*, 4025–4035.

Nagy, A., Rossant, J., Nagy, R., Abramow-Newerly, W., and Roder, J.C. (1993). Derivation of completely cell culture-derived mice from early-passage embryonic stem cells. Proc. Natl. Acad. Sci. USA *90*, 8424–8428.

Nguyen, H.T., Dalmasso, G., Yan, Y., Laroui, H., Dahan, S., Mayer, L., Sitaraman, S.V., and Merlin, D. (2010). MicroRNA-7 modulates CD98 expression during intestinal epithelial cell differentiation. J. Biol. Chem. *285*, 1479–1489.

Paraskevopoulou, M.D., Georgakilas, G., Kostoulas, N., Reczko, M., Maragkakis, M., Dalamagas, T.M., and Hatzigeorgiou, A.G. (2013). DIANA-LncBase: experimentally verified and computationally predicted microRNA targets on long non-coding RNAs. Nucleic Acids Res. *41*, D239–D245.

Pauli, A., Norris, M.L., Valen, E., Chew, G.L., Gagnon, J.A., Zimmerman, S., Mitchell, A., Ma, J., Dubrulle, J., Reyon, D., et al. (2014). Toddler: an embryonic signal that promotes cell movement via Apelin receptors. Science *343*, 1248636.

Quinlan, A.R., and Hall, I.M. (2010). BEDTools: a flexible suite of utilities for comparing genomic features. Bioinformatics *26*, 841–842.

Redmer, T., Diecke, S., Grigoryan, T., Quiroga-Negreira, A., Birchmeier, W., and Besser, D. (2011). E-cadherin is crucial for embryonic stem cell pluripotency and can replace OCT4 during somatic cell reprogramming. EMBO Rep. *12*, 720–726.

Rinn, J.L., and Chang, H.Y. (2012). Genome regulation by long noncoding RNAs. Annu. Rev. Biochem. *81*, 145–166.

Robinson, M.D., McCarthy, D.J., and Smyth, G.K. (2010). edgeR: a Bioconductor package for differential expression analysis of digital gene expression data. Bioinformatics *26*, 139–140.

Royce-Tolland, M.E., Andersen, A.A., Koyfman, H.R., Talbot, D.J., Wutz, A., Tonks, I.D., Kay, G.F., and Panning, B. (2010). The A-repeat links ASF/SF2-dependent Xist RNA processing with random choice during X inactivation. Nat. Struct. Mol. Biol. *17*, 948–954.

Rugg-Gunn, P.J., Cox, B.J., Lanner, F., Sharma, P., Ignatchenko, V., McDonald, A.C., Garner, J., Gramolini, A.O., Rossant, J., and Kislinger, T. (2012). Cell-surface proteomics identifies lineage-specific markers of embryo-derived stem cells. Dev. Cell *22*, 887–901.

Schratt, G., Philippar, U., Berger, J., Schwarz, H., Heidenreich, O., and Nordheim, A. (2002). Serum response factor is crucial for actin cytoskeletal organization and focal adhesion assembly in embryonic stem cells. J. Cell Biol. *156*, 737–750.

Singh, A.M., Hamazaki, T., Hankowski, K.E., and Terada, N. (2007). A heterogeneous expression pattern for Nanog in embryonic stem cells. Stem Cells *25*, 2534–2542.

Sigova, A.A., Mullen, A.C., Molinie, B., Gupta, S., Orlando, D.A., Guenther, M.G., Almada, A.E., Lin, C., Sharp, P.A., Giallourakis, C.C., et al. (2013). Divergent transcription of noncoding RNA/mRNA gene pairs in embryonic stem cells. Proc. Natl. Acad. Sci. USA *110*, 2876–2881.

Tang, F., Hajkova, P., Barton, S.C., Lao, K., and Surani, M.A. (2006). MicroRNA expression profiling of single whole embryonic stem cells. Nucleic Acids Res. *34*, e9.

Tani, H., Mizutani, R., Salam, K.A., Tano, K., Ijiri, K., Wakamatsu, A., Isogai, T., Suzuki, Y., and Akimitsu, N. (2012). Genome-wide determination of RNA stability reveals hundreds of short-lived noncoding transcripts in mammals. Genome Res. *22*, 947–956.

Tazawa, H., Yano, S., Yoshida, R., Yamasaki, Y., Sasaki, T., Hashimoto, Y., Kuroda, S., Ouchi, M., Onishi, T., Uno, F., et al. (2012). Genetically engineered oncolytic adenovirus induces autophagic cell death through an E2F1-microRNA-7-epidermal growth factor receptor axis. Int. J. Cancer *131*, 2939–2950.

Trapnell, C., Pachter, L., and Salzberg, S.L. (2009). TopHat: discovering splice junctions with RNA-Seq. Bioinformatics *25*, 1105–1111.

Ulitsky, I., Shkumatava, A., Jan, C.H., Sive, H., and Bartel, D.P. (2011). Conserved function of lincRNAs in vertebrate embryonic development despite rapid sequence evolution. Cell *147*, 1537–1550.

Wang, K.C., and Chang, H.Y. (2011). Molecular mechanisms of long noncoding RNAs. Mol. Cell *43*, 904–914.

Wang, Y., Xu, Z., Jiang, J., Xu, C., Kang, J., Xiao, L., Wu, M., Xiong, J., Guo, X., and Liu, H. (2013). Endogenous miRNA sponge lincRNA-RoR regulates Oct4, Nanog, and Sox2 in human embryonic stem cell self-renewal. Dev. Cell *25*, 69–80.

Wapinski, O., and Chang, H.Y. (2011). Long noncoding RNAs and human disease. Trends Cell Biol. *21*, 354–361.

White, J., and Dalton, S. (2005). Cell cycle control of embryonic stem cells. Stem Cell Rev. *1*, 131–138.

Wickham, H. (2009). ggplot2: Elegant Graphics for Data Analysis (Springer Science & Business Media).

Willems, E., Leyns, L., and Vandesompele, J. (2008). Standardization of real-time PCR gene expression data from independent biological replicates. Anal. Biochem. *379*, 127–129.

Xie, D., Chen, C.C., Ptaszek, L.M., Xiao, S., Cao, X., Fang, F., Ng, H.H., Lewin, H.A., Cowan, C., and Zhong, S. (2010). Rewirable gene regulatory networks in the preimplantation embryonic development of three mammalian species. Genome Res. *20*, 804–815.

Xu, H., Ang, Y., Sevilla, A., Lemischka, I.R., and Ma'ayan, A. (2014). Construction and validation of a regulatory network for pluripotency and self-renewal of mouse embryonic stem cells. PLoS Comput. Biol. *10*, e1003777.

Ying, Q.L., Wray, J., Nichols, J., Batlle-Morera, L., Doble, B., Woodgett, J., Cohen, P., and Smith, A. (2008). The ground state of embryonic stem cell self-renewal. Nature *453*, 519–523.

Yue, F., Cheng, Y., Breschi, A., Vierstra, J., Wu, W., Ryba, T., Sandstrom, R., Ma, Z., Davis, C., Pope, B.D., et al. (2014). A comparative encyclopedia of DNA elements in the mouse genome. Nature *515*, 355–364.

Zhang, C., and Darnell, R.B. (2011). Mapping in vivo protein-RNA interactions at single-nucleotide resolution from HITS-CLIP data. Nat. Biotechnol. *29*, 607–614.

Zhang, H., Cai, K., Wang, J., Wang, X., Cheng, K., Shi, F., Jiang, L., Zhang, Y., and Dou, J. (2014). MiR-7, inhibited indirectly by LincRNA HOTAIR, directly inhibits SETDB1 and reverses the EMT of breast cancer stem cells by downregulating the STAT3 pathway. Stem Cells *32*, 2858–2868.

Zhong, S., Joung, J., Zheng, Y., Chen, Y., Liu, B., Shao, Y., Xiang, J.Z., Fei, Z., and Giovannoni, J.J. (2011). High-throughput Illumina strand-specific RNA sequencing library preparation. Cold Spring Harb. Protoc. *2011*, 940–949.

Stem Cell Reports, Volume *9*

Supplemental Information

Long Noncoding RNA Moderates MicroRNA Activity to Maintain Self-Renewal in Embryonic Stem Cells

Keriayn N. Smith, Joshua Starmer, Sarah C. Miller, Praveen Sethupathy, and Terry Magnuson

FIGURE S1

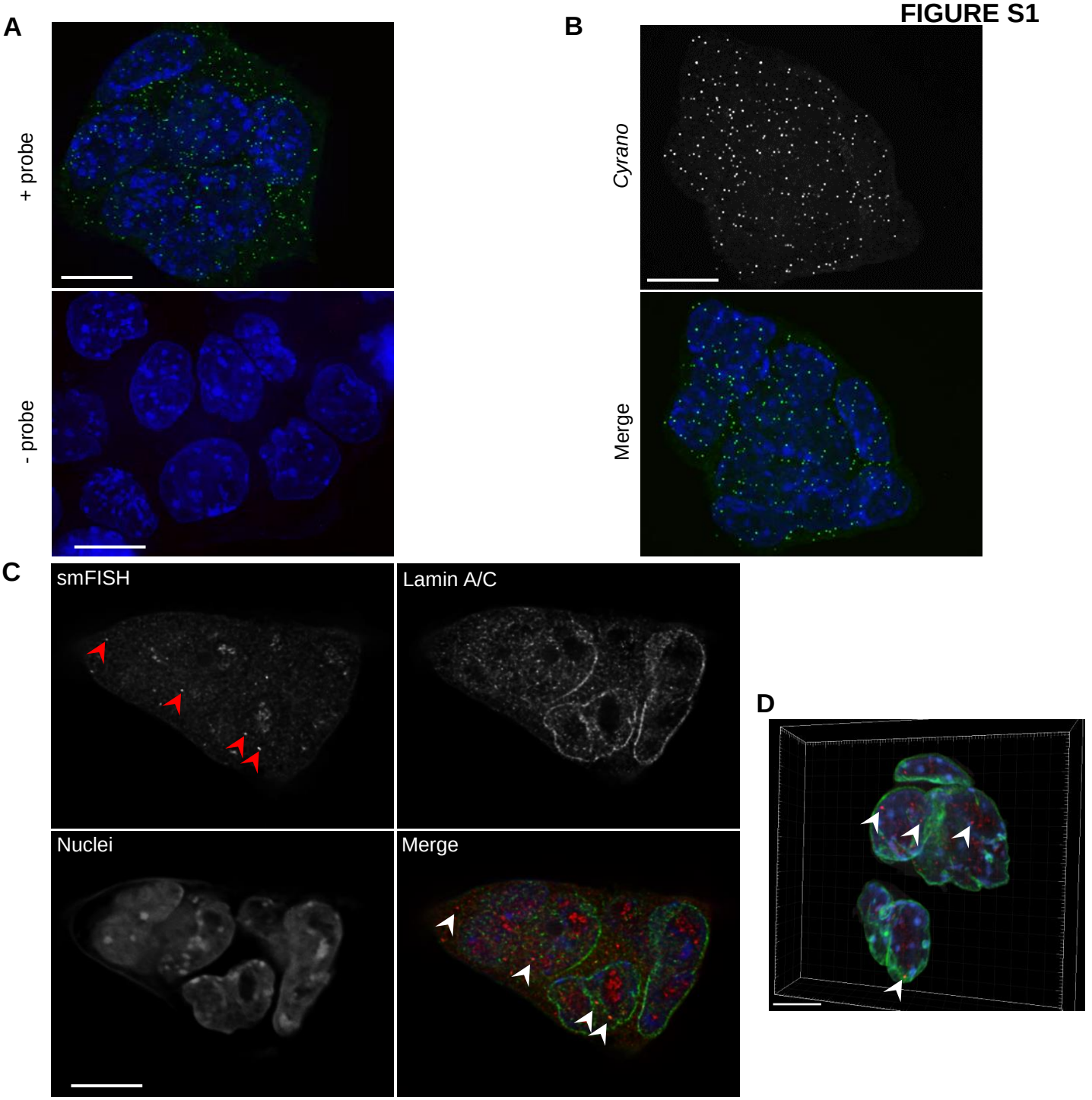
A
+ probe
- probe
B
Cyrano
Merge
C
smFISH
Lamin A/C
Nuclei
Merge
D
E
Human ES cells
Scale
10 kb
hg19
chr15:
41,590,000
OIP5-AS1
Ensembl Genes
H1hSC cel pA- + 2
H1hSC cel pA+ + 2
H1hSC nuc pA- + 2
H1hSC nuc pA+ + 2
H1hSC cyt pA- + 2
H1hSC cyt pA+ + 2

FIGURE S2

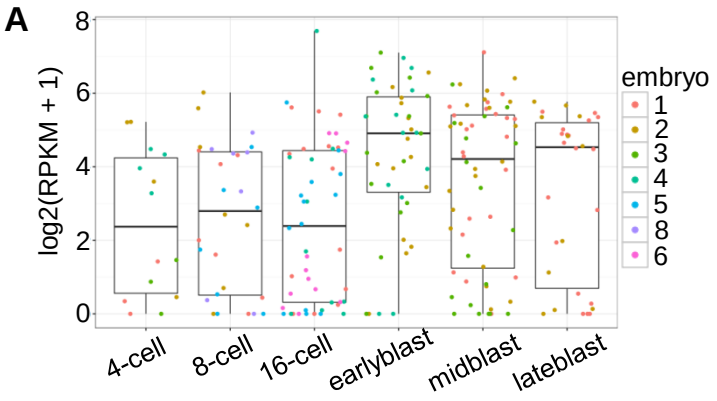
A
log2(RPKM + 1)
embryo
1
2
3
4
5
8
6
4-cell
8-cell
16-cell
earlyblast
midblast
lateblast

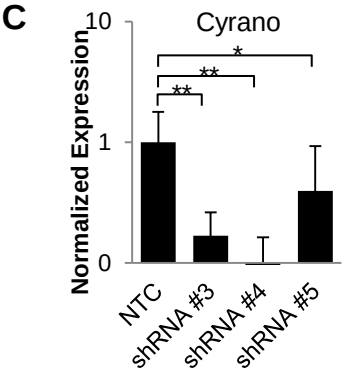
C
Cyrano
Normalized Expression
NTC
shRNA #3
shRNA #4
shRNA #5

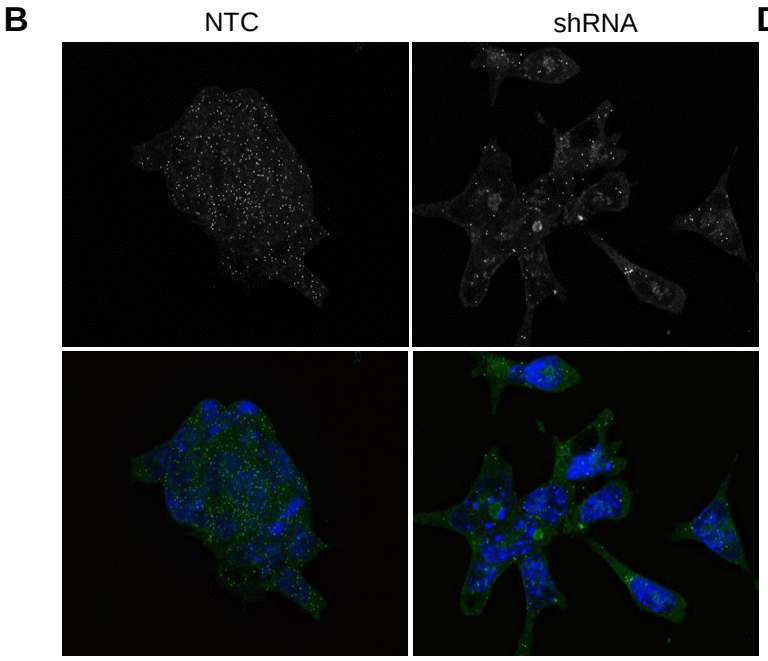
B
NTC
shRNA

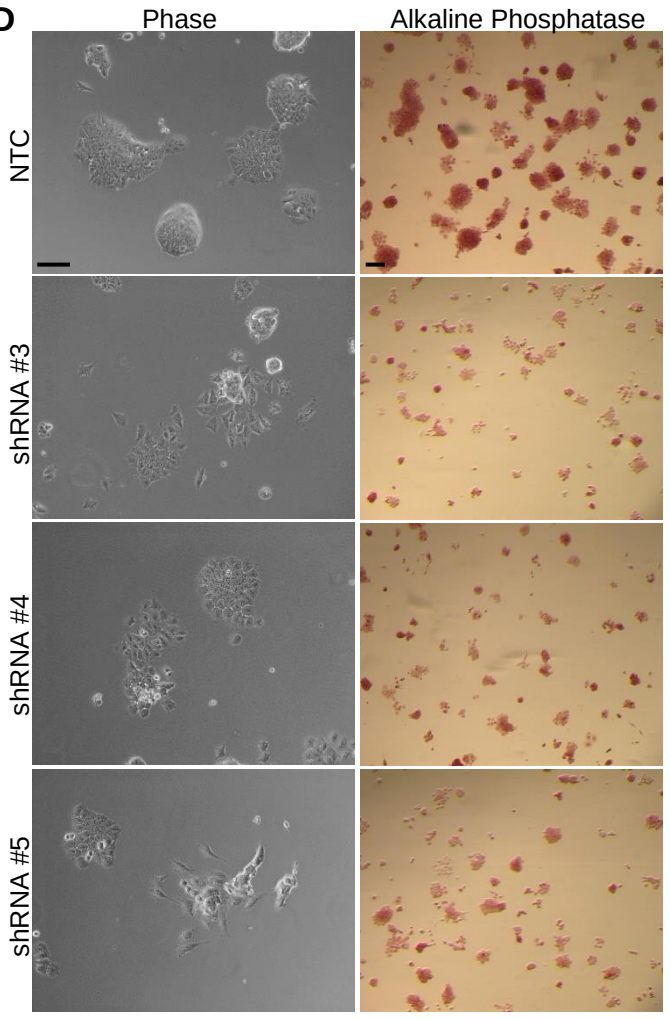
D
Phase
Alkaline Phosphatase
NTC
shRNA #3
shRNA #4
shRNA #5

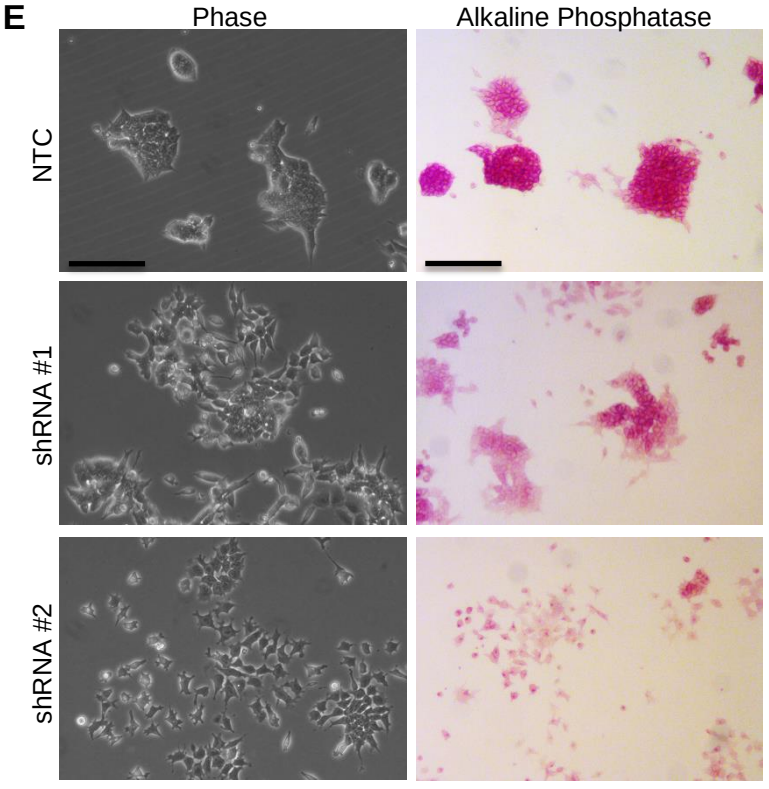
E
Phase
Alkaline Phosphatase
NTC
shRNA #1
shRNA #2

FIGURE S3

A

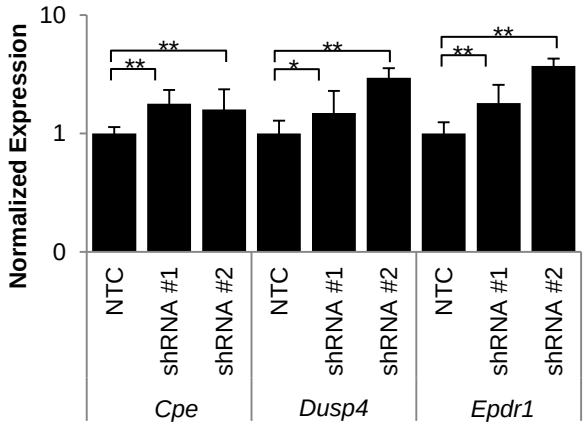
Normalized Expression
10
1
0
**
**
**
*
**
**
NTC
shRNA #1
shRNA #2
NTC
shRNA #1
shRNA #2
NTC
shRNA #1
shRNA #2
Cpe
Dusp4
Epdr1

B

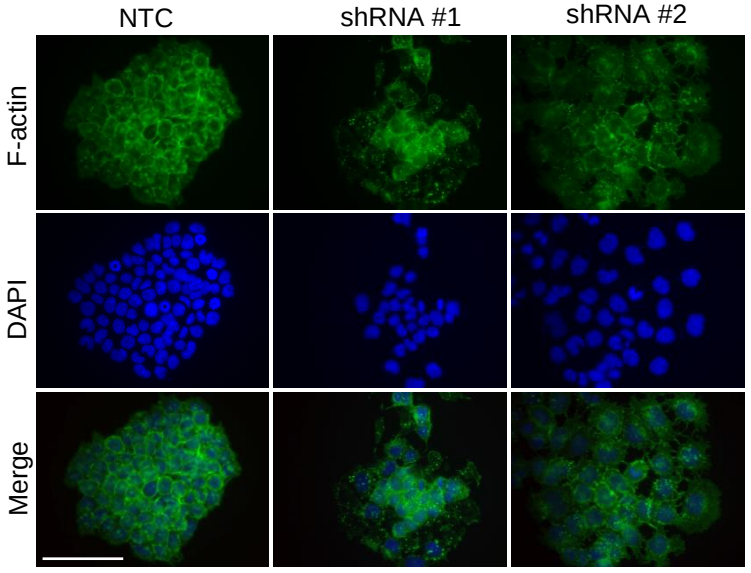
NTC
shRNA #1
shRNA #2
F-actin
DAPI
Merge

FIGURE S4

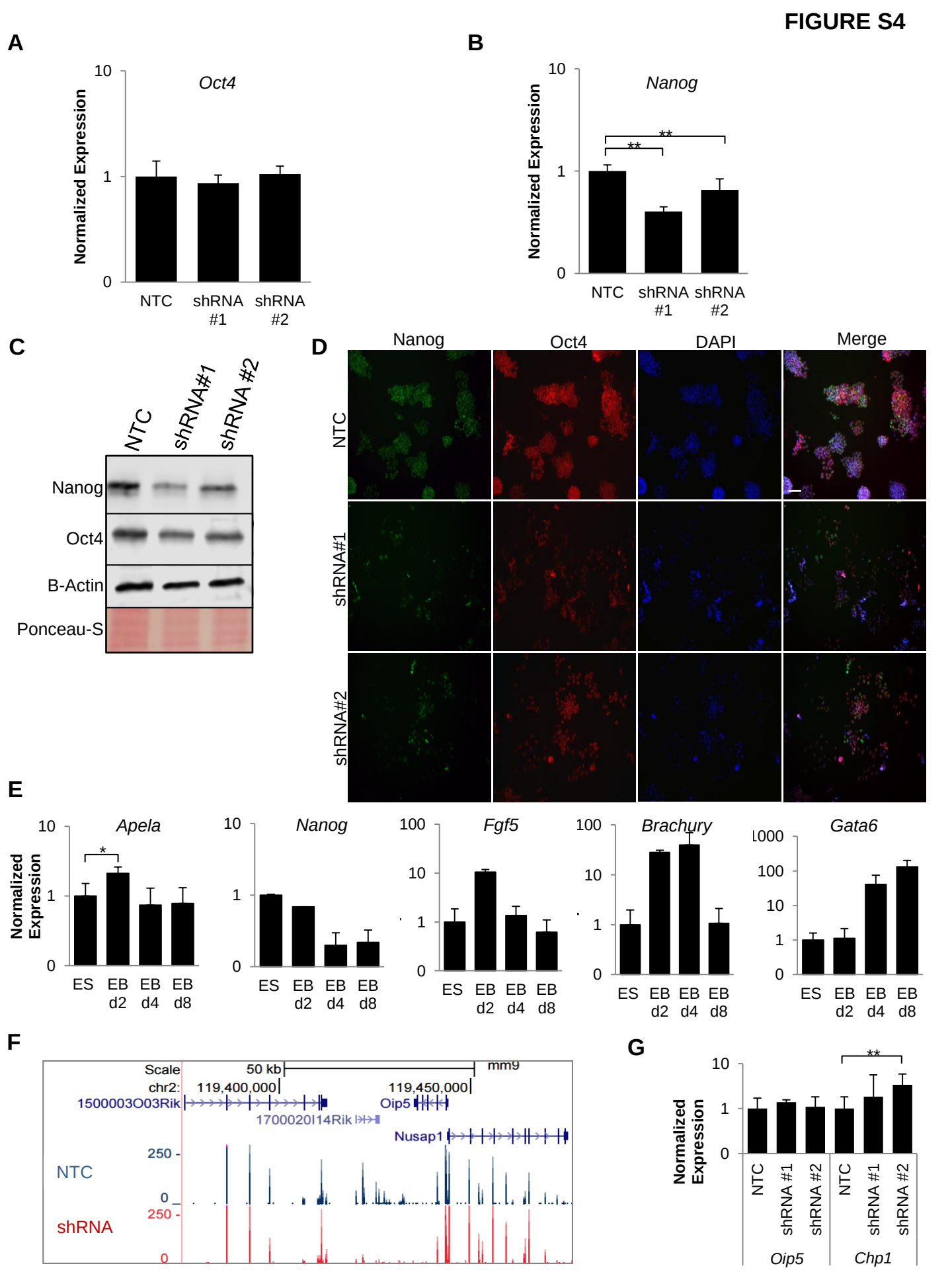
A
Oct4
Normalized Expression
10
1
0
NTC
shRNA #1
shRNA #2
B
Nanog
Normalized Expression
**
**
C
NTC
shRNA#1
shRNA #2
Nanog
Oct4
B-Actin
Ponceau-S
D
Nanog
Oct4
DAPI
Merge
NTC
shRNA#1
shRNA#2
E
Apela
Nanog
Fgf5
Brachury
Gata6
Normalized Expression
ES
EB d2
EB d4
EB d8
F
Scale
50 kb
mm9
chr2:
119,400,000
119,450,000
1500003O03Rik
Oip5
1700020I14Rik
Nusap1
NTC
shRNA
250
0
G
Normalized Expression
**
NTC
shRNA #1
shRNA #2
Oip5
Chp1

FIGURE S5

A

Ensembl Transcript ID	Transcript name	Seed length	Start	End
ENSMUST00000153581	***1700020I14Rik-001***	***8***	***2959***	***2952***
ENSMUST00000147425	*1700020I14Rik-002*	8	606	599
ENSMUST00000153581	***1700020I14Rik-001***	***7***	***2958***	***2952***
ENSMUST00000147425	*1700020I14Rik-002*	7	605	599

B

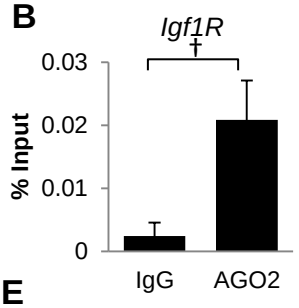

C

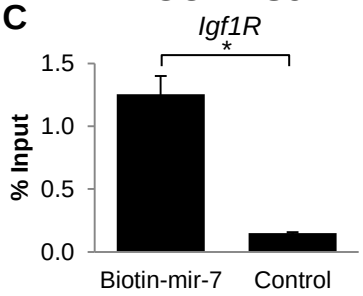

D

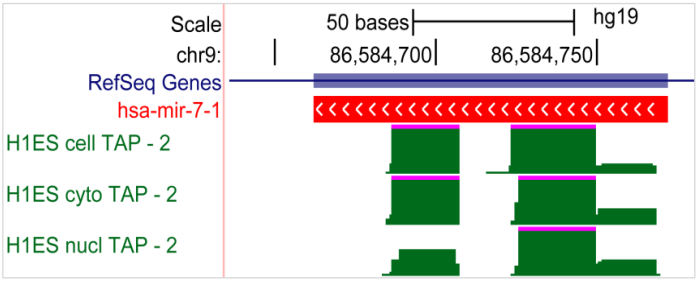

E

Gene	RefSeq ID	Algorithms	Region
Itga9	NM_133721	6/7	3′ UTR
Itga9	NM_001113514	4/7	3′ UTR
Itga9	NM_133721	4/7	CDS
Itga9	NM_001113514	2/7	CDS
Nanog	NM_028016	6/7	3′ UTR
Nanog	NM_028016	3/7	CDS

F

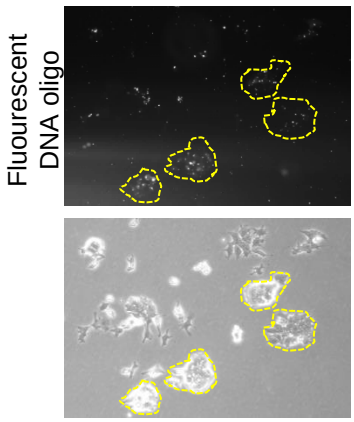

G

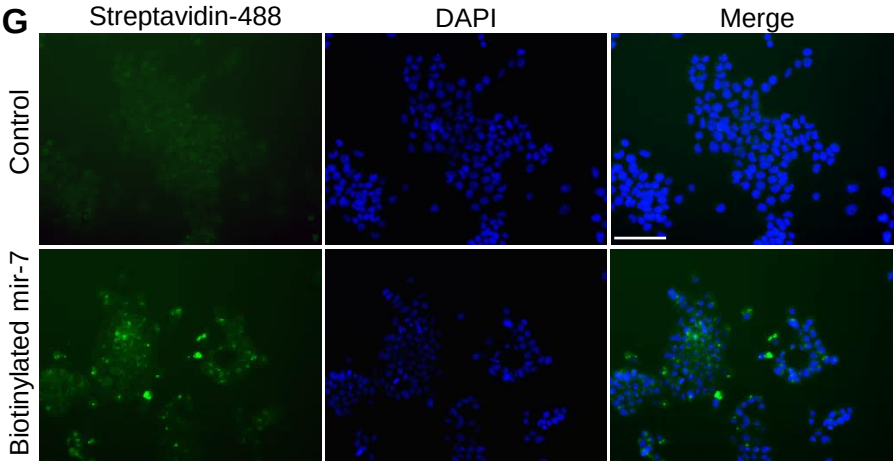

H

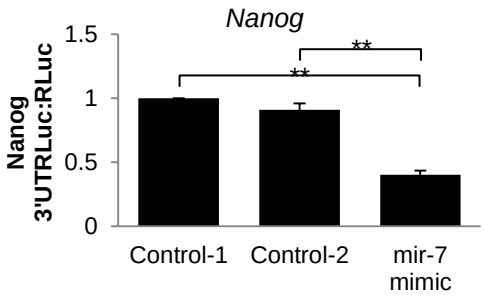

I

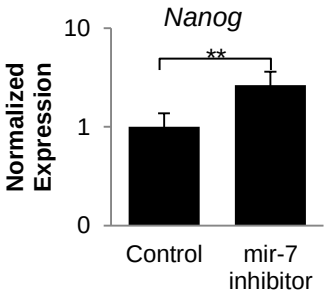

J

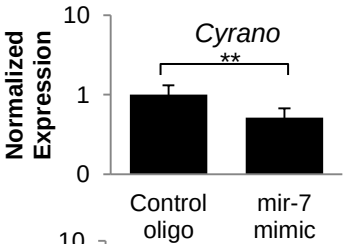

K

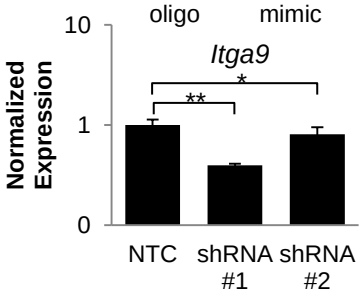

FIGURE S6

A

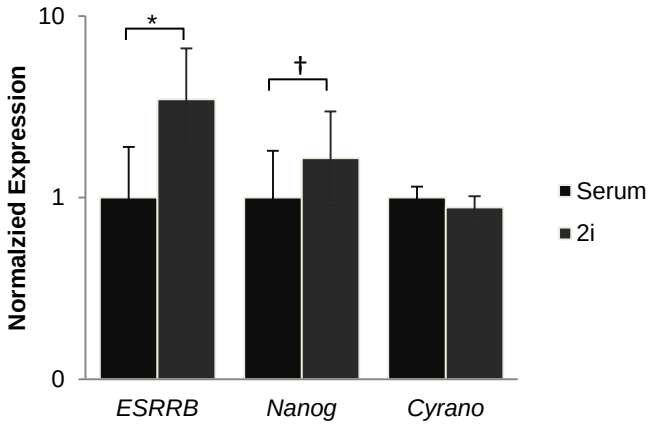

Figure S1, Related to Figure 1. Subcellular localization of *Cyrano*. (A) Specificity of the smFISH probe used to detect *Cyrano* in R1 mouse ES cells. Nuclei are shown in blue (DAPI); Scale bar, 10 μm. (B) Similar subcellular localization of *Cyrano* is observed by smFISH in ES 2-1 mouse ES cells. Nuclei are shown in blue (DAPI); Scale bar, 10 μm. (C) Immunofluorescence at a position of 5.2μm within an ES cell colony, using a lamin A/C antibody to localize the nuclear periphery, coupled with smFISH and DAPI staining confirmed the presence of smFISH signals (red arrowheads for contrast, left upper panel; white arrowheads, right lower panel) in the nucleus as well as the cytoplasm. (D) 3D reconstruction of nuclear volume only, indicates a fraction of *Cyrano* molecules localize to the nucleus (white arrowheads); Scale bar, 3 μm. (E) UCSC genome browser plots illustrating RNA-Seq results which indicate *Oip5-AS1's (Cyrano*'s ortholog) expression and subcellular localization in human ES cells.

Figure S2, Related to Figure 2. Embryonic Expression and Independent Validation of *Cyrano* knockdown and phenotype. (A) Single cell RNA-Seq analysis (GSE45719) of *Cyrano*, in pre-implantation development. (B) Significant reduction in *Cyrano* expression is confirmed with smFISH. Independent knockdown using three additional shRNAs (C). Experiments were performed in triplicate, normalized to *GAPDH*, with error bars representing 95% CI. This confirms reduction in the capacity to maintain self-

renewing ES cell colonies upon *Cyrano* loss (D). (E) Independent validation of the *Cyrano*-deficient phenotype in the ES 2-1 ES cell line.

Figure S3, Related to Figure 3. Gene expression analysis and differential colony structure upon *Cyrano* knockdown. (A) qRT-PCR validation of the differentially expressed non-pluripotency related genes *Cpe*, *Dusp4* and *Epdr1* (approximate positions circled in Fig. 3A) after *Cyrano* knockdown. Experiments were performed in triplicate, normalized to *GAPDH*, with error bars representing 95% CI. *p<0.05, **p<0.01. (B) Immunofluorescence examination of phalloidin staining to examine F-actin localization in control and knockdown cells. Nuclei, blue (DAPI); Scale bar, 100 μm. Data are from 3 independent experiments.

Figure S4, Related to Figure 4. Aberrant gene expression suggests *Cyrano* functions in trans to impact ES cell self-renewal. qRT-PCR monitoring of *Oct3/4* (A) and *Nanog* (B) levels upon *Cyrano* knockdown. Experiments were performed in triplicate, normalized to *GAPDH*, with error bars representing 95% CI. (C-D) Significant decreases in NANOG protein levels occur with *Cyrano* KD. (E) Assessment of *Apela* expression in embryoid body differentiation relative to marker gene expression. Experiments were performed in triplicate, normalized to *GAPDH*, with error bars

representing 95% CI. (F-G) No significant and consistent changes in expression are seen for neighboring genes (*Oip5* and *Chp1/1500003O03Rik)* of *Cyrano*. Experiments were performed in triplicate, normalized to *GAPDH*, with error bars representing 95% CI. *p<0.05, **p<0.01. Data are from 3 independent experiments.

Figure S5, Related to Figure 5. Regulatory loop involving *Cyrano* and *mir-7.* (A) Positions of seed sequences in *Cyrano* as identified by miRWalk (the position corresponding to the conserved atypical mir-7 binding sequence is bold). See Table S1 for further details. *Note, despite not being called by miRWalk, the additional *mir-7* seed can also be found in the *1700020I14Rik*-001 isoform (approximate nucleotide position, 768; blue box in Figure 5A). (B) RNA-immunoprecipitation showing the *mir-7* target *Igf1R* being bound by Ago2 in ESCs. Experiments were performed in triplicate with error bars representing S.E.M. (C) miRNA pulldown and qPCR indicates a physical interaction between *Igf1R* and *mir*-7 in ESCs, with experiments performed in triplicate and error bars representing S.E.M. (D) UCSC genome browser plot showing subcellular localization of *mir-7,* similar to *Cyrano* (see Figure S1E). (E) Number of algorithms as assessed by miRWalk which identify mir-7 seed sequences in *Itga9* and *Nanog.* Transfections with a fluorescent DNA oligo (F) and biotinylated *mir-7* (G) were used to elucidate the success of *mir-7* transfection in ES cells. (H) Despite having only a

7mer-A1 seed sequence, *mir-7* inhibited luciferase activity based on the *Nanog* 3'UTR. Experiments were performed in triplicate, error bars represent S.E.M. (I) *mir-7* inhibition increases *Nanog* levels. (J) *mir-7* overexpression reduces *Cyrano* levels. (K) *Itga9* levels decrease with *Cyrano* knockdown. Experiments were performed in triplicate, normalized to *GAPDH*, with error bars representing 95% CI. Data are from 3 independent experiments. *$p<0.05$, **$p<0.01$, $^{\dagger}p<0.1$.

Figure S6, Related to Figure 6. Examination of *Cyrano* in 2i+LIF medium. (A) No significant changes are seen in *Cyrano* levels in 2i medium relative to serum containing medium. Experiments were performed in triplicate, normalized to *GAPDH*, with error bars representing 95% CI. Data are from 3 independent experiments. *$p<0.05$, $^{\dagger}p<0.1$.

Table S1, Related to Figure 5. Table S1 provides a summary of lncRNA targets of *mir-7.* SPMS: Starting Position of a miRNA seed; SL: Seed length; SeedS: Seed start; SeedE: Seed end.

Table S2, Related to Figure 5. Table S2 provides a summary of miRNA site predictions in the 3'UTR and CDS of Itga9 and Nanog as provided by miRWalk which includes

assessments using the following algorithms: miRWalk, Microt4, miRanda, PITA, RNA22, RNAhybrid and Targetscan. The 'SUM' column indicates how many algorithms were able to identify the miRNA target site.

Table S3, Oligos used in this study

Supplemental Experimental Procedures

Cell Culture and RNAi

Mouse R1 (XY, Nagy et al., 1993) ESCs were maintained in Dulbecco's Modified Eagle Medium supplemented with 10% FBS, 10% Knockout Serum Replacement, 2mM L-glutamate, 1mM sodium pyruvate, 0.1mM β-mercaptoethanol, and 100U/ml penicillin-streptomycin and LIF on gelatin-coated dishes. Mouse ES2-1 cells (XX, Royce-Tolland et al., 2010) were maintained in Dulbecco's Modified Eagle Medium supplemented with 15% FBS, 2mM L-glutamate, 1mM sodium pyruvate, 0.1mM β-mercaptoethanol, 1x MEM non-essential amino acids,100U/ml penicillin-streptomycin and LIF on feeders or gelatin-coated dishes. Embryoid body differentiation was carried out on low adherent dishes under LIF withdrawal conditions.

Apoptosis was monitored using the ReadyProbes Cell Viability Imaging Kit two days post-transfection (ThermoFisher).

Cyrano cDNA was obtained from the RIKEN cRNA collection (Source BioScience, clone ID M5C1004K09), transferred to pCAGEN or pCAGIG (Gift from Connie Cepko, Addgene plasmid #11159) and transfected into ESCs using Lipofectamine LTX reagent (ThermoFisher). Similarly, shRNA constructs in pSicoR-Ef1a-mCh-Puro (Gift from Bruce Conklin, Addgene plasmid # 31845) (Salomonis et al., 2010), pSicoR PGK puro (Gift from Tyler Jacks, Addgene plasmid # 12084) (Ventura et al., 2004) or SmartVector (ThermoFisher) targeting *Cyrano* and non-targeting control were transfected into ESCs using Lipofectamine LTX reagent (ThermoFisher), followed by selection/enrichment upon passaging at d1 post-transfection using puromycin selection or flow cytometry at the UNC Flow Cytometry Core Facility to enrich for transfectants. Alternatively, lentiviral particles at a MOI of 50-100 were used. Cell death assays were carried out without selection at d2 post-transfection. Gene expression assays were carried out upon selection on d2 and d3 post-transfection and phenotypic assays including morphological assessments and alkaline phosphatase activity determination were carried out on d3 post-transfection.

miR-7 overexpression was carried out using the Lipofectamine RNAiMax reagent and the mmu-miR-7a-5p miRIDIAN microRNA mimic (Dharmacon) compared to control

oligos, (Dharmacon, ThermoFisher), while inhibition was carried out with a mmu-miR-7a-5p inhibitor (Dharmacon).

RNA Extraction and Quantitative RT-PCR

To investigate RNA stability, actinomycin D (10µg/ml) was added to cell culture medium and cells incubated for the stated periods.

To prepare nuclear and cytoplasmic fractions, ESCs were incubated in hypotonic buffer (10mM HEPES, 10mM KCl, 0.1mM EDTA, 0.1mM EGTA), 1mM DTT and protease inhibitors. NP-40 (1.6%) was added and the sample vortexed briefly and centrifuged to pellet nuclei, which permitted removal of the cytoplasmic supernatant. Nuclear proteins were extracted from the pellet with 20mM HEPES, 0.4M NaCl, 1mM EDTA, 1mM EGTA, 1mM DTT and protease inhibitors.

smFISH

A pool of FISH probes, comprising 36 20-mer probes that show complementarity to *Cyrano* were designed with the Stellaris Probe designer. Hybridization was carried out according to the manufacturer's recommendations (Biosearch Technologies). Briefly, cells were cultured on coverslips for approximately 24-30h before colonies became

densely structured to enable visualization of individual cells. Cells were fixed with 4% PFA in PBS and permeabilized with 70% ethanol for 1 hr at 4°C. After incubation in wash buffer (10% formamide, 2xSSC), cells were hybridized in 100mg/ml dextran sulphate, 1% formamide and 2xSSC overnight at 37°C. Slides were subsequently submerged in wash buffer twice for 30 min at 37°C, followed by a brief incubation in 2xSSC.

To enable visualization of the nuclear periphery, immunofluorescence to detect lamin A/C localization was carried out prior to FISH described above. After fixing with 4% PFA in PBS and permeabilizing with 0.5% Triton-X100/PBS for 10 min at room temperature, primary antibody incubations were carried out for 1hr at room temperature followed by washes and incubation with fluorescent-conjugated Alexa Fluor secondary antibodies for 1h at room temperature (ThermoFisher). After washes, a post-fix step was carried out for 10 min at room temperature using 4% PFA in PBS prior to washing with wash buffer in preparation for FISH. Coverslips were mounted with Prolong Gold Antifade Mountant containing DAPI (ThermoFisher) for nuclear visualization. Z-stack images were acquired by AxioVision software, using a 63x or 100x objective on a Zeiss Axio Imager 2, and deconvolution carried out using an iterative-constrained algorithm. Imaris (Bitplane) was used for 3D reconstruction and surface reconstruction of the nucleus to

enable specific identification of the nuclear volume (Hooker Imaging Core, University of North Carolina at Chapel Hill).

Quantitation of smFISH signals was carried out using the StarSearch software (Raj Laboratory, University of Pennsylvania). The average count per cell was derived by the total number of FISH signals/colony relative to the total number of cells as determined by non-overlapping DAPI stained nuclei.

Transcriptomics

Libraries for RNA-Seq were prepared using 30 µg total RNA with a modified dUTP Strand Specific method (Zhong et al., 2011) from cells three days post-knockdown with shRNA#1. Poly A+ selection was carried out using Dynabeads (ThermoFisher), and RNA fragmentation carried out with the Ambion Fragmentation reagent (ThermoFisher) for 4 min at 70 ºC. Fragmented RNA was purified using the RNA Clean and Concentrator Kit (Zymo), and used for first strand synthesis with Superscript III (ThermoFisher) and random primers (NEB). After purification with the RNA Clean and Concentrator Kit (Zymo), second strand synthesis with dUTP was carried out for 2h at 16 ºC. End repair (NEBNext Kit), purification with 1.8 volumes of Ampure beads (Beckman-Coulter), followed by A-tailing with Klenow exo- and purification with 1.8 volumes of Ampure beads, followed by standard Illumina Library preparation. Here,

adapters were ligated using the Quick Ligation Module (NEBNext Kit). Libraries were purified twice with Ampure beads (1 volume, followed by 0.8 volumes), followed by amplification, uracil-DNA glycosylase treatment and quantitation for submission at the University of North Carolina at Chapel Hill High Throughput Sequencing Facility. qPCR validation was carried out on independent samples with both shRNA #1 and shRNA #2.

Western blot Analysis & Immunofluorescence

Antibodies were used for lamin A/C (E-1, Santa Cruz), Oct4 (H10, Santa Cruz), Nanog (A300-397A, Bethyl Laboratories; 8822, Cell Signaling Technologies) and e-Cadherin (13-1900, Zymed). Cell extracts for immunoblot analysis were prepared using a modified RIPA buffer (50mM Tris pH 8.0, 150mM NaCl, 1% NP40, 0.5% deoxycholate, 0.1% SDS, dithothreitol) containing protease inhibitors (Roche), electrophoresed and blotted onto a nitrocellulose/PVDF membrane (BioRad) before incubation in the appropriate primary antibody. After incubation with HRP-conjugated secondary antibody (Santa Cruz), membranes were developed with SuperSignal West Dura Chemiluminescent substrate (Pierce).

In immunofluorescence experiments, cultured cells were fixed with 4% PFA in PBS and permeabilized with 0.3% Triton-X100/PBS for 5 min at room temperature. After blocking

for 1 hr, primary antibody incubations were carried out for 1hr at room temperature or overnight at 4°C, followed by washes and incubation in fluorescent-conjugated Alexa Fluor secondary antibodies (ThermoFisher). DAPI (ThermoFisher) was used for nuclear visualization.

Supplemental References

Murakami, K., Araki, K., Ohtsuka, S., Wakayama, T., and Niwa, H. (2011). Choice of random rather than imprinted X inactivation in female embryonic stem cell-derived extra-embryonic cells. Development *138,* 197-202.

Rosengren, L., Vasilcanu, D., Vasilcanu, R., Fickenscher, S., Sehat, B., Natalishvili, N., Naughton, S., Yin, S., Girnita, A., Girnita, L., *et al.* (2006). IGF-1R tyrosine kinase expression and dependency in clones of IGF-1R knockout cells (R-). Biochem. Biophys. Res. Commun. *347*, 1059-1066.

Salomonis, N., Schlieve, C.R., Pereira, L., Wahlquist, C., Colas, A., Zambon, A.C., Vranizan, K., Spindler, M.J., Pico, A.R., Cline, M.S.*, et al.* (2010). Alternative splicing regulates mouse embryonic stem cell pluripotency and differentiation. Proc. Natl. Acad. Sci. U. S. A. *107,* 10514-10519.

Ventura, A., Meissner, A., Dillon, C.P., McManus, M., Sharp, P.A., Van Parijs, L., Jaenisch, R., and Jacks, T. (2004). Cre-lox-regulated conditional RNA interference from transgenes. Proc. Natl. Acad. Sci. U. S. A. *101,* 10380-10385.